PHYSIOLOGICALY BASED PHARMACOKINTEIC MODELLING OF 18F-DCFPYL TO PREDICT THE TISSUE DISTRIBUTION IN PATIENTS WITH PROSTATE CANCER

HABIBE YILMAZ (4267583) - AUTHOR

SUZANNE VAN DER GAAG & IMKE BARTELINK - DAILY SUPERVISORS

HARRY HENDRIKSE - REFEREE

VERA DENEER – EXAMINER

ABSTRACT

Introduction: The goal of this study was to develop a whole body physiological based pharmacokinetic-model (PBPK-model) to predict the tissue distribution of 18F-DCFPyL in patients with prostate cancer (PCa).

Method: The model was extended from a previously published PBPK-model describing PCa patients to predict the tissue distribution of 18F-DCFPyL. This model describes the tumors and organs at risks. The model was simulated and the results were compared to literature observations of patients with metastatic PCa.

Results: Our model adequately predicted the distribution of 18F-DCFPyL. Sensitivity analysis showed that the receptor densities, tumor flow and haematocrit had significant influence on the model outcome. The release and degradation of 18F-DCFPyL, and total organ volumes showed no significant influence on the outcome.

Discussion: The tumor flow, receptor densities and haematocrit should be measured in the future to accurately predict tissue distribution. The release and degradation of 18F-DCFPyL, and total organ volumes can be fixed on literature data.

Conclusion: The final PBPK-model was able to adequately predict tissue distribution of 18F-DCFPyL.

Keywords PSMA, 18F-DCFPyL, Prostate cancer, physiologically based pharmacokinetic model, theranostics

INTRODUCTION

Prostate cancer (PCa) is the most common malignancy in men and causes 1-2% of deaths in this part of the population. (1) One of the hallmarks of PCa is the overexpression of the type II transmembrane enzymatic protein prostate specific membrane antigen (PSMA). (2, 3) This makes PSMA a valuable target for imaging and therapy with radiolabelled PSMA-targeting ligands as these ligands will accumulate in the PSMA-positive PCa lesions. (3) Aside from malignant tissue, PSMA is also physiologically expressed on the prostate, proximal tubule cells in the kidney, spleen, liver, small intestine, colon, ganglial cells in the gastrointestinal-tract, parotid glands, submandibular glands and lacrimal glands. (4-9) Expression in healthy tissues is lower than in malignant tissues but it is nonetheless important because it makes them potential organs at risk (OARs) due to tracer accumulation. (3)

Various radioisotopes can be used to label PSMA-targeting ligands. The positron-emitters fluor-18 and gallium-68 can be used for imaging while the beta-emitters like lutetium-177 and alpha-emitters like actinium-225 can be used for therapy. (10, 11) Radio-isotopes are coupled to high affinity PSMA-ligands, such as DCFPyL. (10)

Dosing for imaging and therapeutic PSMA-ligands is provided as an one dose fits all. In the case of imaging ligands, such as 18F-DCFPyL and 68Ga-PSMA 11, a dose of 111 to 370 MBq is administered. (12, 13) Whereas, therapeutic radioligands, such as 177Lu-PSMA, are given in higher dosages (6 to 7.4 GBq), extracted from 177Lu-dotatate for neuroendocrine tumors. (14, 15) At standard dosing, the absorbed radiation dose in target tissue (prostate and tumors) and OARs may vary between patients. (16, 17) Previous literature states that high tumor burden will lead to more tumor uptake and less OAR uptake. (18)

Due to the specific targeting mechanism, some patients experience adverse effects due to therapy. The most common adverse effect is xerostomia and was reported in up to 30% of the patients. (19) This happens due to radioactive tracer uptake in the salivary glands. Other less frequent adverse effects are anaemia, leukopenia, thrombocytopenia, liver transaminase elevation, fatigue and pain. (20) Another interesting adverse effect is toxicity in the kidneys. Currently, have been conducted with patients who have an advanced disease progression. Therefore, the long-term effects of these adverse effects are yet unknown. In the future, when PSMA therapy is used in earlier stages of PCa, long-term kidney toxicity will need to be avoided. (16, 19) Aside from adverse events, it is reported that there is a possible correlation between response and disease markers such as total tumor volume (TTV) and PSMA expression. (16, 21) This calls for the use of dose-optimization such as personalized dosing. A way to incorporate patient characteristics to

create a personalized dosing scheme is through a whole body physiologically based pharmacokinetic model (PBPK-model). (22) PBPK-models take patient characteristics such as weight, height, eGFR and more disease specific parameters such as PSMA receptor density or TTV into account. A PBPK-model can also simulate the distribution and delivered radiation dose to target organs and OARs. This makes it possible to calculate the optimal dosage for each specific patient, based on their own characteristics. (18)

A PBPK-model is a mechanistic and physiological multi-compartment model which described the drug distribution over time. PBPK-model specific parameters are flow (F_i) between the blood pool and the organs, organ volume (V_i) and tissue permeability (PS_i). Whereas target affinity (k_{on}, k_{off}, k_D) and elimination are drug specific parameters. (23) Expansion of the model by including receptor binding kinetics is relevant for modelling of PSMA-targeting ligands such as 18F-DCFPyL. 18F-DCFPyL is a small molecular PSMA-ligand with a high PSMA affinity and is excreted renally. Potential OARs for 18F-DCFPyL are the kidneys, lacrimal- and salivary glands, red marrow and lungs. (13, 24, 25) By incorporation of the known patient and drug specific predictors of PK into a PBPK-model, the model can be used to quantify variability in uptake in tumor and OARs and develop strategies for personalized dosing regimens.

We hypothesize that a PBPK-model is sufficient to predict the tissue distribution of 18F-DCFPyL. The goal of this study was to develop a whole body PBPK-model to predict the tissue distribution of 18F-DCFPyL in patients with PCa. Ultimately such a model can be used for personalized dosing of PSMA-targeted radioligand therapy as a part of theranostics.

METHOD

A whole body PBPK-model was developed to predict the tissue distribution of 18F-DCFPyL. A schematic representation of the whole body PBPK-model and the sub compartmental model for PSMA-positive tissues (tumor, prostate, liver, spleen and gastrointestinal tract) are shown in figures 1A and 1B. Equations for the model and figures for other tissues are shown in the supplemental data (Supplementary figure 1A-E and supplementary equations 1-16). The final model described the flow of drug amount in nanomoles from arteries to the vascular space of the organ (F_i). From the vascular space it can diffuse to the interstitial space (PS_i). In PSMA-positive tissues the drug can bind to and dissociate from PSMA-receptors on the cell surface (K_{on} or k_{off}). Receptor bound ligand can then be internalized into the cells ($\lambda_{int,i}$). Internalized ligand is degraded and released by the cells ($\lambda_{rel,\ i}$).

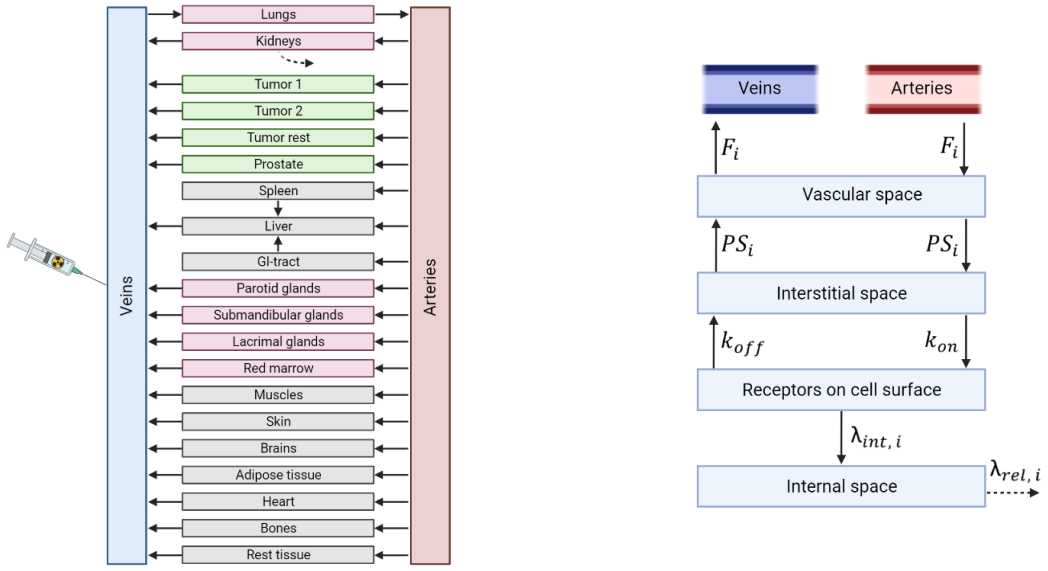

A **B**

Figure 1. A) Schematic representation of the final PBPK-model structure. The drug is injected into venous compartment. From here it can distribute to the lungs and from the lungs to the arterial compartment. The drug can then be distributed to the other tissue compartments. The target tissues are coloured green; the OARs are coloured red; the other tissues are coloured grey. **B) A schematic representation of the sub compartments of a PSMA-positive organ.** The flow in and out of the vascular space is described by the organ flow F_i. The movement between the vascular and interstitial space is described by the permeability surface product PS_i. The association to and dissociation from the PSMA-receptors on cell surface are described by the k_{on} and k_{off}. The internalisation is described by $\lambda_{int,i}$, whereas the degradation and release is described by $\lambda_{rel,i}$.

MODELLING

BASE MODEL SELECTION

As a basis the whole body PBPK-model created by Begum *et al* was used. (18) The base PBPK-model structure described the distribution of PSMA ligands 68Ga-PSMA HBED-CC and 177Lu-PSMA I&T. This model was an extensive whole body PBPK-model and included separate compartments for the tumors and prostate. It also included separate compartments for the OARs (lungs, kidneys, parotids- and submandibular glands, lacrimal glands and red marrow). The remaining organs were the muscles, skins, adipose tissue, brains and rest tissue. The base model was rebuild and its performance was evaluated for the PSMA ligands used by Begum *et al*. After it showed a correct prediction, the model was adapted to create an accurate prediction of 18F-DCFPyL tissue distribution and provide information on variability in PK among patients. Extensions to the model were made to adapt the model to reflect the pharmacokinetic processes involved in the distribution and elimination of 18F-DCFPyL in the tissues of interest. These include the renal filtration and excretion, target affinity and receptor recycling which were based on information found in literature. Radioactive decay of PSMA-ligand was not included in our model, because tissue distribution of 18F-DCFPyL in prostate cancer patients is corrected for physical decay. (26) The most important components and adaptations to the model are described below.

KIDNEY MODEL

The kidney model was a physiological model which used the eGFR to describe the excretion of 18F-DCFPyL. Figure x below shows a schematic representation of the model. Equations 1, 2 and 3 show the differential equations used for the kidney model. As the figure shows, the drug first enters the vascular space of the kidney. From here it can be filtrated through the eGFR to the kidney lumen. This filtration is described by the term $F_{fil} * \left(\frac{A_{vasc,\ kid}}{V_{vasc,\ kid}}\right)$ in equation 1. In the kidney lumen, the drug can bind to PSMA receptors on the surface of proximal tubule cells and be internalized. This is described by the term $\left(k_{on} * A_{lum,kid} * \frac{RF_{kid}}{V_{lum,kid}}\right)$ in equation 2. Drug that isn't bound to the PSMA receptors is excreted into the urine. This is described by the term $\left(F_{ex} * \left(\frac{A_{int,\ i}}{V_{int,\ i}}\right)\right)$ in equation 3.

$\frac{dA_{vasc,\ kid}}{dt} = F_{kid} * \frac{A_{art}}{V_{art}} - F_{kid} * \left(\frac{A_{vasc,\ kid}}{V_{vasc,\ kid}}\right) - F_{fil} * \left(\frac{A_{vasc,\ kid}}{V_{vasc,\ kid}}\right)$	(Eq. 1)
$\frac{dA_{lum,kid}}{dt} = F_{fil} * \left(\frac{A_{vasc,\ kid}}{V_{vasc,\ kid}}\right) - F_{ex} * \left(\frac{A_{lum,kid}}{V_{lum,kid}}\right) - \left(k_{on} * A_{lum,kid} * \frac{RF_{kid}}{V_{lum,kid}}\right) + k_{off} * AR_{kid}$	(Eq. 2)
$\frac{dAR_{kid}}{dt} = \left(k_{on} * A_{lum,kid} * \frac{RF_{kid}}{V_{lum,kid}}\right) - k_{off} * AR_{kid} - \lambda_{int,\ kid} * AR_{kid}$	(Eq. 3)

FREE RECEPTOR MODEL

Two compartments were used to describe the PSMA binding in PSMA-positive organs to describe change in the amount of free available PSMA-receptors over time (Equation 4 and 5, and Supplemental figure 4). Equation 4 was based on the model reported by Winter *et al* (27) and is the direct inverse to the amount of receptor bound ligand, AR_i (equation 5). RF_i describes the amount of unbound receptors (equation 4). The baseline amount of receptors (RF_i) available for drug binding was calculated with V_i and $R_{dens,\ i}$. Following bolus injection of 18F-DCFPyL into the model, the free receptor amount decreases by association of ligand to receptor $\left(k_{on} * A_{int,i} * \frac{RF_i}{V_{int,\ i}}\right)$, increases by dissociation of ligand from receptor $\left(k_{off} * AR_i\right)$ and decreases through internalization of receptor-ligand complex $\left(\lambda_{int,\ i} * AR_i\right)$.

In this model, two assumptions were made. Firstly, the model assumes that there is no physiological synthesis or degradation of receptors. Secondly, the model assumes that after internalization or receptor-ligand complex, the receptor is uncoupled from ligand and recycled to the cell surface without a delay in time.

$\frac{dRF_i}{dt} = k_{off} * AR_i - \left(k_{on} * A_{int,i} * \frac{RF_i}{V_{int,\ i}}\right) + \lambda_{int,\ i} * AR_i$	(4)
$\frac{dAR_i}{dt} = \left(k_{on} * A_{int,i} * \frac{RF_i}{V_{int,\ i}}\right) - k_{off} * AR_i - \lambda_{int,\ i} * AR_i$	(5)

PARAMETERS

The model parameters are described in supplementary table 1. The physiological parameters such as organ volumes and flow were not expected to differ between healthy and PCa patients or between different kinds of ligands. For this reason, these parameters were calculated based on or taken from literature. Drug specific parameters were adapted to 18F-DCFPyL. The most important changes are described below.

RECEPTOR BINDING

Receptor binding values, K_D and K_{on} were taken from literature. (26, 28) The k_{off} was calculated by dividing multiplying the k_{on} with the K_D.

KIDNEY PARAMETERS

Some of the kidney parameters were changed to fit 18F-DCFPyL. Firstly, it was assumed that 18F-DCFPyL was fully excreted by the glomerular filtration. This was based on the molecular weight of 18F-DCFPyL. (29) Secondly, it was assumed that once filtrated, 18F-DCFPyL would not be reabsorbed through tubular reabsorption. The short half-life of 18F-DCFPyL (3.47 h) and low blood concentration after 120 minutes suggest the drug is not reabsorbed. (24, 26)

SENSITIVITY ANALYSIS

A local sensitivity analysis was done for 25 different patient specific parameters to determine the robustness of our model and the influence of these parameters to predict interindividual variability in drug uptake between patients. The deviation from the average was calculated with equation 6. The mean, upper and lower limit of each parameter was based on literature data or taken from the patients included in the studies by Janssen *et al (2019 & 2020)*. (26, 30) (supplementary table 2). A new simulation was performed for each separate deviation from the baseline value. Only one parameter was changed at a time, which resulted in 54 separate simulations. For each simulation the deviation from average was calculated for the tumors, and presented using waterfall plots. A deviation above 20% was seen as clinically significant. Supplementary table 2 shows the parameter values.

$$Deviation\ from\ mean = mean\left(\frac{Deviation - Average}{Deviation}\right) * 100 \quad \text{(Eq. 6)}$$

PATIENT DATA

To determine whether the PBPK-model could accurately predict the tissue distribution of 18F-DCFPyL in prostate cancer patients, the data was compared with observed PET-scan data of 8 patients with metastatic prostate cancer previously presented in Amsterdam UMC (REF). The PET-scan data gave information on activity in blood, tumor lesion, muscles and lungs between 5 and 120 minutes after injection, measured using the SUV_{peak}. All patients were included in a previously reported study. (26, 30) The age, bodyweight (BW), body height (BH), eGFR and haematocrit (H) of these patients was also acquired for a proper fit.

SOFTWARE AND SIMULATIONS

Software used for the modelling and simulations was R in R Studio (version 4.0.3). To solve the ODEs, the deSolve package (version 1.32) was used. (31, 32)

Simulations were performed at a time range of 0-120 minutes with a time interval of 1 minute, reflecting the PK-profile during sampling of the clinical study data. 18F-DCFPyL was administered (in the model and clinical practice) via single bolus injection to the venous compartment. (24)

RESULTS

FINAL MODEL VALIDATION

The predictive value of the final model was evaluated by reproducing the reported values of patient 4 reported by Begum *et al*. (18) Two separate simulations were performed for 68Ga and 177Lu. The final model adequately reproduced the literature data (supplementary figure 2 and 3). As a result the model was deemed fit to implement for 18F-DCFPyL.

FINAL MODEL

The tissue distribution of 18F-DCFPyL in patients with PCa was simulated with the full PBPK-model to predict the concentration in the arterial blood, total tumor lesion, lungs and muscles. The result of the simulation is shown in figures 2A-D. The means of the BW, BH, eGFR, age and H were used. Supplemental figure 4A-H show the simulations for specific patients.

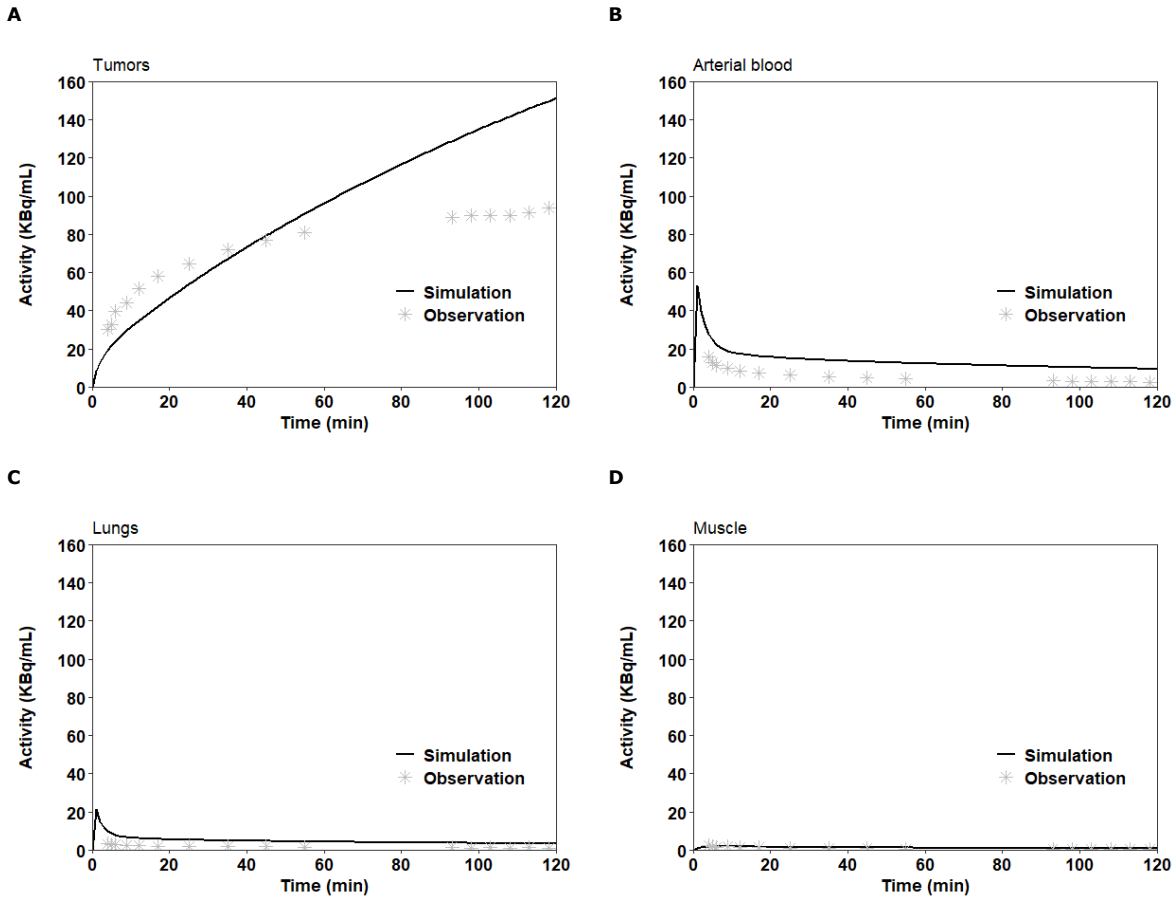

Figure 2. The simulation together with the corresponding observations (26) for the tumors (A), arterial blood (B), lungs (C) and muscles (D). The simulations are representing with solid black lines. The observations are represented with grey stars.

Figure 2B shows that the PBPK-model could adequately predict the distribution in tumors, arterial blood, lungs and muscles. The blood, lung and muscle simulations showed a slight over prediction of the C_{max} compared to the observed values. The tumor simulation shows a steeper slope than the observations. It also does not seem to reach plateau within 120 minutes, in contrast to the observations.

Sensitivity analysis

A local sensitivity analysis was performed for 25 different parameters. The results of the sensitivity analysis are shown in figure 3 and supplementary figure 5A-G.

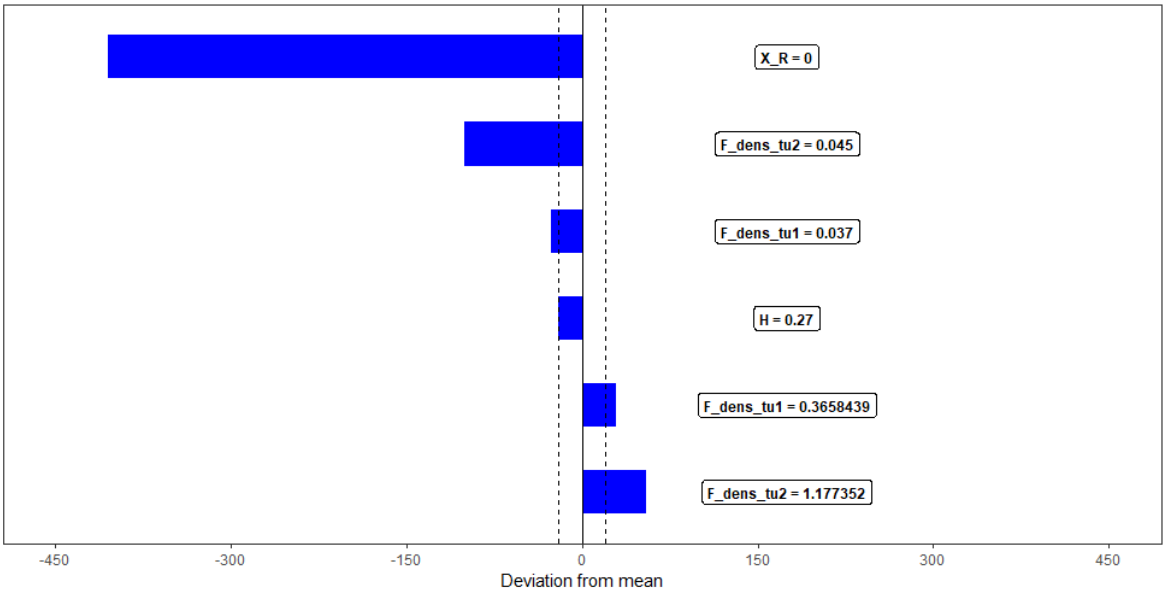

Figure 3. The waterfall plot of the sensitivity analysis for the X_R, $F_{dens,tu1}$, $F_{dens,tu1}$ and H. The 20% deviation from the mean is represented by the dotted black line.

The parameters in figure 3 showed a 20% deviation from the mean. These were the parameters X_R, $F_{dens,tu2}$, $F_{dens,tu1}$ and H. The tumor flow densities for tumors 1 and 2 showed significance for both the lower and upper values. Other parameters that didn't show significance are given in supplementary figure 5.

DISCUSSION

In this study a whole body PBPK-model was developed to predict the tissue distribution of 18F-DCFPyL in patients with PCa. Data about the height, weight, eGFR, age and haematocrit of specific patients were used to create individual patient-predictions. Other parameters were taken from literature. The model is mechanistic and is able to predict the distribution in different organs, including target tissues and OARs. A receptor binding model was added to describe the amount of free receptors available in the PSMA-positive organ compartments. The kidney model was adapted to accurately describe the excretion of 18F-DCFPyL. The final model was able to adequately predict the distribution of 18F-DCFPyL in patients with prostate cancer. Our tumor concentration predictions did not show a maximal tumor uptake within 120 minutes, whereas observations showed saturation.

A local sensitivity analysis was performed to study the robustness of our model and the influence of different patient or drug specific characteristics. The analysis was done on 25 different parameters. The sensitivity analysis proved the robustness of our model, as only 4 parameters (X_r, the $F_{dens,tu1}$, $Fd_{ens,tu2}$ and H) caused a deviation higher than 20%. The influence of haematocrit on the tumor uptake has not been reported yet. Interestingly, our study population had an average haematocrit of 0.37 whereas literature shows an average between 0.40-0.55 (supplementary table 1 and 2). The sensitivity analysis also showed that changes in tumor blood flow significantly influenced the tumor uptake. It is known from literature that tumor blood flow might also be correlated with PCa aggressiveness. (33) Other parameters that showed an almost significant deviation were BW, eGFR, X_v, $R_{dens,tu1}$ and $R_{dens,tu2}$. These results prove that measurements of these parameters are needed to properly predict the tissue distribution with our model. The $\lambda_{rel,kid}$ and $\lambda_{rel,tu}$ showed almost no influence on the model outcome. Thus, these parameters can be fixed on the same literature values in the future and individual estimates are not needed. The organ volumes of the kidneys, parotid-, submandibular-, lacrimal glands liver and spleen showed little effect on the tumor uptake. In the future, the volume of these organs can be calculated from the BW or fixed on literature values instead of measuring them through CT.

Although the model we created showed an accurate fit, there were a few limitations to our study. Firstly, the current receptor model assumes that internalized ligand is directly recycled to the surface. However recycling may be delayed. (27) Secondly, the PSMA receptor densities were taken from literature values. These parameters were not measured in the patient population included by Janssen *et al*. (26) As shown in the sensitivity analysis, these parameters influence the distribution to the tumors. PSMA receptor density is also known to be influenced by androgen depletion therapy. (34) Therefore, this

parameter should be taken from inpatient measurements in the future, to accurately tissue distribution. This could be done through biopsies. (35, 36) Thirdly, the TTVs were not available for the specific patients. Because of this a mean TTV from Janssen *et al* (30) was used for the model. As shown in the sensitivity analysis, this parameter also influences the outcome and should there be measured in individual patients in the future. Lastly, the reported data from Janssen *et al* (26) is from one patient. To study variability between patients it is important to include multiple patients in the future.

Our model is able to adequately predict the tissue distribution of 18F-DCFPyL in patients with prostate cancer. In the future the model should be expanded to include a more accurate receptor model. When radiolabelled PSMA ligands are used for therapy the radiolabelled ligand may cause receptor degradation. This may cause a delay in recycling. This degradation is described in the PSMA-receptor model created by Winter *et al*. This model also includes other factors that influence the receptor amount such as constitutive endocytosis, ligand induced endocytosis, ligand dependent and independent synthesis, ligand independent and independent degradation, and recycling of ligand bound receptors. (27)

Additionally, tumor shrinkage is not accounted for in this model as during the 120 minute simulation time, no changes in tumor volume occur. However, in theranostics, the drug is not just provided for diagnosis, but also for therapy. Therapy with a 177Lu PSMA-ligand is given in cycles of 6-8 weeks, (37) where tumor shrinkage is expected upon rescan. This could also influence the absorbed dosage for the target tissues and the OARs per therapy/scan cycle. (16, 18) For this reason tumor shrinkage is an important addition to future models for therapeutic ligands. A model as such has been created by Kletting *et al*. This model incorporates the parameters volume at time of first PET/CT, net growth rate of androgen-independent cells, biologically effective dose to organs and the intrinsic radio sensitivity of PSMA-positive tumor cells to calculate tumor growth or reduction after 6 weeks of 177Lu-therapy.

When properly validated, the final PBPK-model provides a first step for model-based individualized dosing (MIPD) and in the development for novel PSMA PET tracers in the future. The model is extensive and simulates distribution to a variety of tissues. In combination with patient specific characteristics such as weight, eGFR and TTV, an optimal dose can be calculated. This dose will be based on optimal efficacy and least amount of toxicity. The model can also distinguish between healthy and malignant prostate tissue through the use of the PSMA receptor density, which is different between healthy and malignant tissue. This could be used to predict novel PET tracers with an optimal tumor-to-background contrast in patients and predict the image quality of the compounds.

CONCLUSION

The goal of our research was to investigate whether a whole PBPK-model can correctly predict the tissue distribution of 18F-DCFPyL in patient with PCa. A whole body PBPK-model was developed for this purpose. The developed model predicted an accurate distribution of 18F-DCFPyL in patients with metastatic PCa.

CONFLICT OF INTEREST

The author declares no conflict of interest.

ACKNOWLEDGEMENTS

First I'd like to thank my supervisors Suzanne van der Gaag, Imke Bartelink and Harry Hendrikse.

Second but not least, I would like to thank my fellow students Julia van den Nieuwendijk, Jemayro Hupsel, Yingxue Li, Ardijana Kabašaj, Shiewanie Raddjoe, Mick van de Plas, Medhat Said and Chi Fong Loo for their help and weekly discussions.

During this project I've learned a lot. Not only about my particular subject but about pharmacokinetic modelling of other drugs as well. I've also learned the sometimes uncertain but eventually fulfilling process of research.

REFERENCES

1. Attard G, Parker C, Eeles RA, Schröder F, Tomlins SA, Tannock I, *et al*. Prostate cancer. The Lancet. 2016;387(10013):70-82.

2. Chang SS. Overview of prostate-specific membrane antigen. Rev Urol. 2004;6 Suppl 10:S13-8.

3. Ruigrok EAM, van Weerden WM, Nonnekens J, de Jong M. The Future of PSMA-Targeted Radionuclide Therapy: An Overview of Recent Preclinical Research. Pharmaceutics. 2019;11(11).

4. Klein Nulent TJW, Valstar MH, de Keizer B, Willems SM, Smit LA, Al-Mamgani A, *et al*. Physiologic distribution of PSMA-ligand in salivary glands and seromucous glands of the head and neck on PET/CT. Oral Surg Oral Med Oral Pathol Oral Radiol. 2018;125(5):478-86.

5. Troyer JK, Beckett ML, Wright GL, Jr. Detection and characterization of the prostate-specific membrane antigen (PSMA) in tissue extracts and body fluids. Int J Cancer. 1995;62(5):552-8.

6. Silver DA, Pellicer I, Fair WR, Heston WD, Cordon-Cardo C. Prostate-specific membrane antigen expression in normal and malignant human tissues. Clin Cancer Res. 1997;3(1):81-5.

7. Mhawech-Fauceglia P, Zhang S, Terracciano L, Sauter G, Chadhuri A, Herrmann FR, *et al*. Prostate-specific membrane antigen (PSMA) protein expression in normal and neoplastic tissues and its sensitivity and specificity in prostate adenocarcinoma: an immunohistochemical study using mutiple tumour tissue microarray technique. Histopathology. 2007;50(4):472-83.

8. Liu H, Moy P, Kim S, Xia Y, Rajasekaran A, Navarro V, *et al*. Monoclonal antibodies to the extracellular domain of prostate-specific membrane antigen also react with tumor vascular endothelium. Cancer Res. 1997;57(17):3629-34.

9. O'Keefe DS, Bacich DJ, Heston WD. Comparative analysis of prostate-specific membrane antigen (PSMA) versus a prostate-specific membrane antigen-like gene. Prostate. 2004;58(2):200-10.

10. Schwarzenboeck SM, Rauscher I, Bluemel C, Fendler WP, Rowe SP, Pomper MG, *et al*. PSMA Ligands for PET Imaging of Prostate Cancer. J Nucl Med. 2017;58(10):1545-52.

11. Sandhu S, Guo C, Hofman MS. Radionuclide Therapy in Prostate Cancer: from standalone to combination PSMA theranostics. J Nucl Med. 2021.

12. FDA. FULL PRESCRIBING INFORMATION 2021 [Available from: https://www.accessdata.fda.gov/drugsatfda_docs/label/2020/212642s000lbl.pdf.

13. FDA. FULL PRESCRIBING INFORMATION 2021 [Available from: https://www.accessdata.fda.gov/drugsatfda_docs/label/2021/214793s000lbl.pdf.

14. Hofman MS, Violet J, Hicks RJ, Ferdinandus J, Thang SP, Akhurst T, *et al*. [177 Lu]-PSMA-617 radionuclide treatment in patients with metastatic castration-resistant prostate cancer (LuPSMA trial): a single-centre, single-arm, phase 2 study. The Lancet Oncology. 2018;19(6):825-33.

15. Fendler WP, Rahbar K, Herrmann K, Kratochwil C, Eiber M. (177)Lu-PSMA Radioligand Therapy for Prostate Cancer. J Nucl Med. 2017;58(8):1196-200.

16. Jackson P, Hofman M, McIntosh L, Buteau JP, Ravi Kumar A. Radiation Dosimetry in (177)Lu-PSMA-617 Therapy. Semin Nucl Med. 2022;52(2):243-54.

17. Nautiyal A, Jha AK, Mithun S, Rangarajan V. Dosimetry in Lu-177-PSMA-617 prostate-specific membrane antigen targeted radioligand therapy: a systematic review. Nucl Med Commun. 2022;43(4):369-77.

18. Begum NJ, Thieme A, Eberhardt N, Tauber R, D'Alessandria C, Beer AJ, *et al*. The Effect of Total Tumor Volume on the Biologically Effective Dose to Tumor and Kidneys for (177)Lu-Labeled PSMA Peptides. J Nucl Med. 2018;59(6):929-33.

19. Emmett L, Willowson K, Violet J, Shin J, Blanksby A, Lee J. Lutetium (177) PSMA radionuclide therapy for men with prostate cancer: a review of the current literature and discussion of practical aspects of therapy. J Med Radiat Sci. 2017;64(1):52-60.

20. Sadaghiani MS, Sheikhbahaei S, Werner RA, Pienta KJ, Pomper MG, Solnes LB, *et al*. A Systematic Review and Meta-analysis of the Effectiveness and Toxicities of Lutetium-177-labeled Prostate-specific Membrane Antigen-targeted Radioligand Therapy in Metastatic Castration-Resistant Prostate Cancer. Eur Urol. 2021;80(1):82-94.

21. Seitzer KE, Seifert R, Kessel K, Roll W, Schlack K, Boegemann M, *et al*. Lutetium-177 Labelled PSMA Targeted Therapy in Advanced Prostate Cancer: Current Status and Future Perspectives. Cancers (Basel). 2021;13(15).

22. Hartmanshenn C, Scherholz M, Androulakis IP. Physiologically-based pharmacokinetic models: approaches for enabling personalized medicine. J Pharmacokinet Pharmacodyn. 2016;43(5):481-504.

23. Peters SA. Physiologically-Based Pharmacokinetic (PBPK) Modeling and Simulations2012.

24. Keam SJ. Piflufolastat F 18: Diagnostic First Approval. Mol Diagn Ther. 2021;25(5):647-56.

25. Szabo Z, Mena E, Rowe SP, Plyku D, Nidal R, Eisenberger MA, *et al*. Initial Evaluation of [(18)F]DCFPyL for Prostate-Specific Membrane Antigen (PSMA)-Targeted PET Imaging of Prostate Cancer. Mol Imaging Biol. 2015;17(4):565-74.

26. Jansen BHE, Yaqub M, Voortman J, Cysouw MCF, Windhorst AD, Schuit RC, *et al*. Simplified Methods for Quantification of (18)F-DCFPyL Uptake in Patients with Prostate Cancer. J Nucl Med. 2019;60(12):1730-5.

27. Winter G, Vogt A, Jimenez-Franco LD, Rinscheid A, Yousefzadeh-Nowshahr E, Solbach C, *et al*. Modelling the internalisation process of prostate cancer cells for PSMA-specific ligands. Nucl Med Biol. 2019;72-73:20-5.

28. Kuo HT, Pan J, Zhang Z, Lau J, Merkens H, Zhang C, *et al*. Effects of Linker Modification on Tumor-to-Kidney Contrast of (68)Ga-Labeled PSMA-Targeted Imaging Probes. Mol Pharm. 2018;15(8):3502-11.

29. Schmidt MM, Wittrup KD. A modeling analysis of the effects of molecular size and binding affinity on tumor targeting. Mol Cancer Ther. 2009;8(10):2861-71.

30. Jansen BHE, Cysouw MCF, Vis AN, van Moorselaar RJA, Voortman J, Bodar YJL, *et al*. Repeatability of Quantitative (18)F-DCFPyL PET/CT Measurements in Metastatic Prostate Cancer. J Nucl Med. 2020;61(9):1320-5.

31. RStudio: Integrated Development for R. [Available from: http://www.rstudio.com/.

32. deSolve: Solvers for Initial Value Problems of Differential Equations ('ODE', 'DAE', 'DDE') [Available from: https://cran.r-project.org/web/packages/deSolve/index.html.

33. Jochumsen MR, Sorensen J, Tolbod LP, Pedersen BG, Frokiaer J, Borre M, *et al*. Potential synergy between PSMA uptake and tumour blood flow for prediction of human prostate cancer aggressiveness. EJNMMI Res. 2021;11(1):12.

34. Vaz S, Hadaschik B, Gabriel M, Herrmann K, Eiber M, Costa D. Influence of androgen deprivation therapy on PSMA expression and PSMA-ligand PET imaging of prostate cancer patients. Eur J Nucl Med Mol Imaging. 2020;47(1):9-15.

35. Hupe MC, Philippi C, Roth D, Kumpers C, Ribbat-Idel J, Becker F, *et al*. Expression of Prostate-Specific Membrane Antigen (PSMA) on Biopsies Is an Independent Risk Stratifier of Prostate Cancer Patients at Time of Initial Diagnosis. Front Oncol. 2018;8:623.

36. Wang X, Ma D, Olson WC, Heston WD. In vitro and in vivo responses of advanced prostate tumors to PSMA ADC, an auristatin-conjugated antibody to prostate-specific membrane antigen. Mol Cancer Ther. 2011;10(9):1728-39.

37. Kratochwil C, Fendler WP, Eiber M, Baum R, Bozkurt MF, Czernin J, *et al*. EANM procedure guidelines for radionuclide therapy with (177)Lu-labelled PSMA-ligands ((177)Lu-PSMA-RLT). Eur J Nucl Med Mol Imaging. 2019;46(12):2536-44.

38. Cheong B, Muthupillai R, Rubin MF, Flamm SD. Normal values for renal length and volume as measured by magnetic resonance imaging. Clin J Am Soc Nephrol. 2007;2(1):38-45.

39. Rowland M TT. Clinical pharmacokinetics and pharmacodynamics. Concepts and applications. : Wolters Kluwer Health.

40. Li W, Sun ZP, Liu XJ, Yu GY. [Volume measurements of human parotid and submandibular glands]. Beijing Da Xue Xue Bao Yi Xue Ban. 2014;46(2):288-93.

41. Bingham CM, Castro A, Realini T, Nguyen J, Hogg JP, Sivak-Callcott JA. Calculated CT volumes of lacrimal glands in normal Caucasian orbits. Ophthalmic Plast Reconstr Surg. 2013;29(3):157-9.

42. Shah DK, Betts AM. Towards a platform PBPK model to characterize the plasma and tissue disposition of monoclonal antibodies in preclinical species and human. J Pharmacokinet Pharmacodyn. 2012;39(1):67-86.

43. Wetzels JF, Kiemeney LA, Swinkels DW, Willems HL, den Heijer M. Age- and gender-specific reference values of estimated GFR in Caucasians: the Nijmegen Biomedical Study. Kidney Int. 2007;72(5):632-7.

44. Clinical Methods: The History, Physical, and Laboratory Examinations. 3rd edition. 3 ed.

45. ICRP Publication 23. Report on the Task Group on Reference Man. Oxford: Pergamon Press; 1975.

SUPPLEMENTAL DATA

PBPK-MODEL

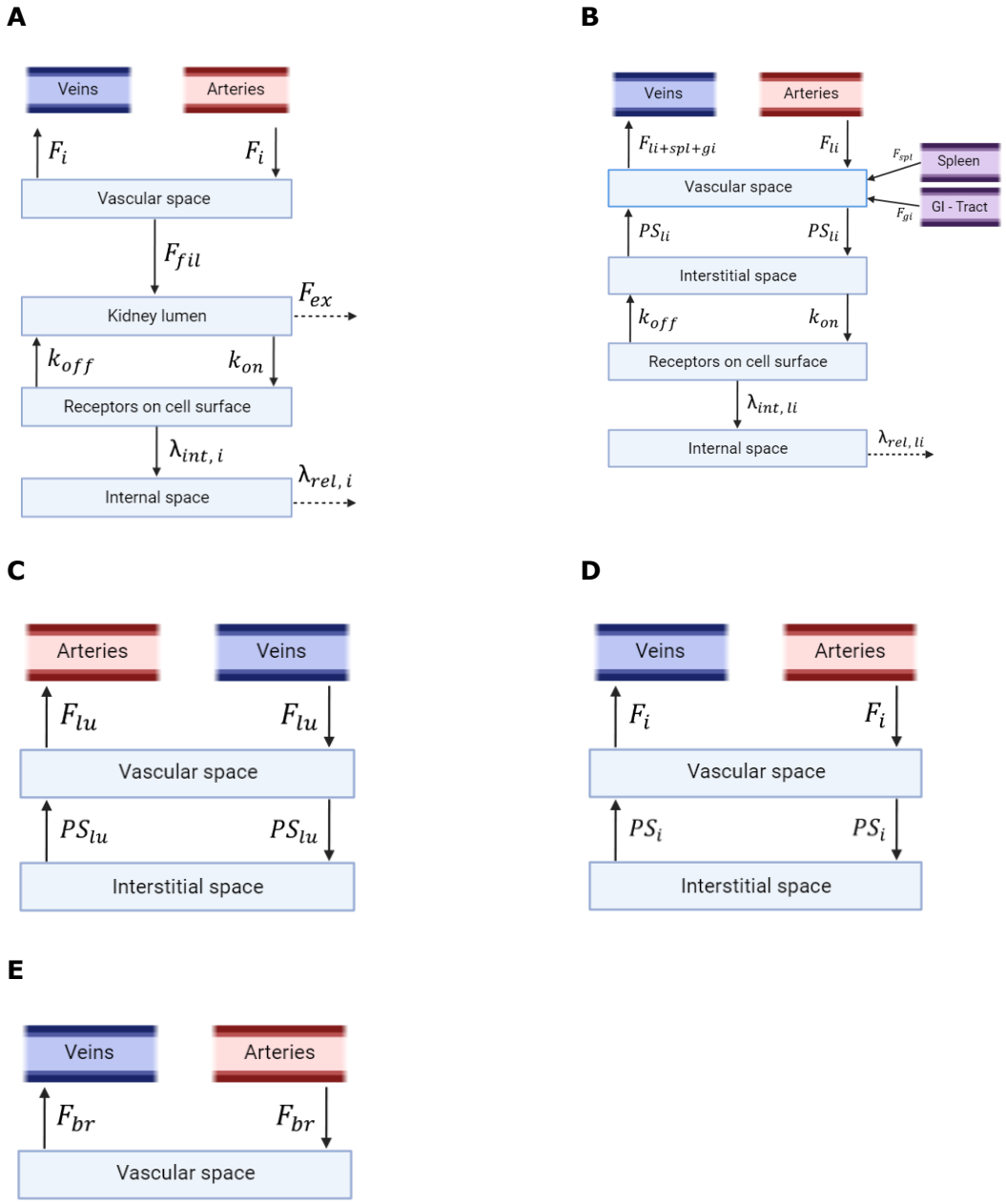

Supplemental figure 1. The models for the sub compartments of the various tissues. A) The sub compartment model of the kidneys. The filtration from the vascular space to the kidney lumen is described by F_{fil}. The excretion from the kidney lumen to the urine is described by F_{ex}. The receptor binding and internalisation is similar to other PSMA-positive tissue model. **B) The sub compartmental model of the liver.** The vascular space receives drug from the arteries (F_{li}), the spleen (F_{spl}) and the GI-tract (F_{GI}). The other compartments are similar to the PSMA-positive tissue model. **C) The compartmental model of the lungs.** The lung receives drug from the veins by F_{lu}. **D) The sub compartmental model of the other PSMA-negative tissues (muscles, adipose, skin, red marrow, bones, rest) except for the brains. E) The sub compartmental model of the brains.** This model only consists of a vascular space as 18F-DCFPyL does not show uptake into the brains. (25)

PBPK-MODEL EQUATIONS

Free vascular ligand

Veins $\frac{dA_{ven}}{dt} = \sum F_i * \frac{A_{vasc,\ i}}{V_{vasc,\ i}} + \left(F_{li+spl+gi}\right) * \frac{A_{vasc,\ li}}{V_{vasc,\ li}} - F_{lu} * \frac{A_{ven}}{V_{ven}}$	Supl. Eq 1
Arteries $\frac{dA_{art}}{dt} = F_{lu} * \frac{A_{vasc,\ lu}}{V_{vasc,\ lu}} - \sum F_i * \frac{A_{art}}{V_{art}}$	Supl. Eq 2
All tissues except lungs, kidneys, liver and brains. $\frac{dA_{vasc,\ i}}{dt} = F_i * \frac{A_{art}}{V_{art}} - F_i * \left(\frac{A_{vasc,\ i}}{V_{vasc,\ i}}\right) - PS_i * \left(\frac{A_{vasc,\ i}}{V_{vasc,\ i}}\right) + PS_i * \left(\frac{A_{int,\ i}}{V_{int,\ i}}\right)$	Supl. Eq 3
Kidneys $\frac{dA_{vasc,\ kid}}{dt} = F_{kid} * \frac{A_{art}}{V_{art}} - F_{kid} * \left(\frac{A_{vasc,\ kid}}{V_{vasc,\ kid}}\right) - F_{fil} * \left(\frac{A_{vasc,\ kid}}{V_{vasc,\ kid}}\right)$	Supl. Eq 4
Lungs $\frac{dA_{vasc,\ lu}}{dt} = F_{lu} * \frac{A_{ven}}{V_{ven}} - F_{lu} * \left(\frac{A_{vasc,\ lu}}{V_{vasc,\ lu}}\right) - PS_{lu} * \left(\frac{A_{vasc,\ lu}}{V_{vasc,\ lu}}\right) + PS_{lu} * \left(\frac{A_{int,\ lu}}{V_{int,\ lu}}\right)$	Supl. Eq 5
Liver $\frac{dA_{vasc,\ li}}{dt} = F_{li} * \frac{A_{art}}{V_{art}} - \left(F_{li+spl+gi}\right) * \frac{A_{vasc,\ li}}{V_{vasc,\ li}} + F_{spl} * \frac{A_{vasc,\ spl}}{V_{vasc,\ spl}} + F_{GI} * \frac{A_{vasc,\ GI}}{V_{vasc,\ GI}} - PS_{li} * \left(\frac{A_{vasc,\ li}}{V_{vasc,\ li}}\right) + PS_{li} * \left(\frac{A_{int,\ li}}{V_{int,\ li}}\right)$	Supl. Eq 6
Brains $\frac{dA_{vasc,\ br}}{dt} = F_{br} * \frac{A_{art}}{V_{art}} - F_i * \left(\frac{A_{vasc,\ br}}{V_{vasc,\ br}}\right)$	Supl. Eq. 8

Free interstitial ligand

PSMA-positive tissues (tumors, prostate, liver, spleen, GI-tract, parotid glands, submandibular glands and lacrimal glands) except for the kidneys $\frac{dA_{int,\ i}}{dt} = PS_i * \left(\frac{A_{vasc,\ i}}{V_{vasc,\ i}}\right) - PS_i * \left(\frac{A_{int,\ i}}{V_{int,\ i}}\right) - \left(k_{on} * A_{int,i} * \frac{RF_i}{V_{int,\ i}}\right) + k_{off} * AR_i$	Supl. Eq. 9
PSMA-negative tissues (red marrow, muscles, skin, brains, adipose tissue, heart, bone and rest) except for brains $\frac{dA_{int,\ i}}{dt} = PS_i * \left(\frac{A_{vasc,\ i}}{V_{vasc,\ i}}\right) - PS_i * \left(\frac{A_{int,\ i}}{V_{int,\ i}}\right)$	Supl. Eq. 10

Free ligand in lumen

$\frac{dA_{lum,kid}}{dt} = F_{fil} * \left(\frac{A_{vasc,\ kid}}{V_{vasc,\ kid}}\right) - F_{ex} * \left(\frac{A_{lum,kid}}{V_{lum,kid}}\right) - \left(k_{on} * A_{lum,kid} * \frac{RF_{kid}}{V_{lum,kid}}\right) + k_{off} * AR_{kid}$	Supl. Eq. 11

Ligand bound to PSMA-receptors on cell-surface

PSMA-positive tissues (tumors, prostate, liver, spleen, GI-tract, parotid glands, submandibular glands and lacrimal glands) except for the kidneys $\frac{dAR_i}{dt} = \left(k_{on} * A_{int,i} * \frac{RF_i}{V_{int,\ i}}\right) - k_{off} * AR_i - \lambda_{int,\ i} * AR_i$	Supl. Eq. 12
Kidneys $\frac{dAR_{kid}}{dt} = \left(k_{on} * A_{lum,kid} * \frac{RF_{kid}}{V_{lum,kid}}\right) - k_{off} * AR_{kid} - \lambda_{int,\ kid} * AR_{kid}$	Supl. Eq. 13

Internalized ligand

All PSMA-positive tissues (kidneys, tumors, prostate, liver, spleen, GI-tract, parotid glands, submandibular glands and lacrimal glands) $\frac{\mathrm{dA_{intern,\ i}}}{\mathrm{dt}} = \lambda_{\mathrm{int,\ i}} * \mathrm{AR_i} - \lambda_{\mathrm{ext,\ i}} * \mathrm{A_{intern,\ i}}$	Supl. Eq. 14

Free receptors on cell surface

All PSMA-positive tissues (tumors, prostate, liver, spleen, GI-tract, parotid glands, submandibular glands and lacrimal glands) except for the kidneys $\frac{dRF_i}{dt} = k_{off} * AR_i - \left(k_{on} * A_{int,i} * \frac{RF_i}{V_{int,\ i}}\right) + \lambda_{int,\ i} * AR_i$	Supl. Eq. 15
Kidneys $\frac{dRF_{kid}}{dt} = k_{off} * AR_{kid} - \left(k_{on} * A_{int,kid} * \frac{RF_{kid}}{V_{lum,kid}}\right) + \lambda_{int,\ kid} * AR_{kid}$	Supl. Eq. 16

PBPK-MODEL PARAMETERS

Supplemental table 1. The parameters used for the PBPK-model.

Parameter	Definition	*Value*	Unit	Source
k_{on}	Association rate	0.09	$\frac{L}{nmol*min}$	(26, 28)
k_{off}	Dissociation rate	$K_{dis} * k_{on} = 0.0441$	Min^{-1}	(26)
K_{dis}	Dissociation constant	0.49 ± 0.04	$\frac{nmol}{L}$	(28)
φ_{Kid}	Sieving of 18F-DCFPYL	*1.0*	Ratio	(29)
Fra_{ex}	Excreted fraction of ligand	*1.0*	Fraction	(24, 26)
Dose	Molar dosage of ligand	$\frac{A_{inj}}{A_{spec}}$	nmol	(26, 30)
A_{Inj}	Activity of administered 18F-DCFPYL	*0.30*	*GBq*	(26, 30)
A_{spec}	Specific activity of 18F-DCFPYL	*0.045*	$\frac{GBq}{nmol}$	(26, 30)
BW	Body weight	*93.25*	Kg	(26)
BH	Body height	*181.5*	cm	(26)
BSA	Body surface area	$0.007184 * BH^{0.725} * BW^{0.425}$	m^2	(18)
eGFR	Estimated glomerular filtration rate	*73.5*	mL/min	(26)
H	Hematocrit	*0.36*	Ratio	(26)
Age	Age	*68.25*	Years	(18)
$V_{tot, bw}$	Total body volume	*BW*	L	(18)
$V_{tot, i}$	Total volume of tissue		L	(18)
$V_{tot, ven}$	Total venous volume	$0.0452 * BW$	L	(23)
$V_{tot, art}$	Total arterial volume	$0.0224 * BW$	L	(23)
$V_{tot, lu}$	Total lung volume	$\frac{BW}{71}$	L	(18)
TTV	Total tumor volume	*0.0214*	L	(18, 30)
$V_{tot, tu1}$	Total volume of tumor 1	$0.02313625 * TTV$	L	(26)
$V_{tot, tu2}$	Total volume of tumor 2	$0.02956298 * TTV$	L	(26)
$V_{tot, turest}$	Total volume of the rest tumor	$0.9473008 * TTV$	L	(26)
X_V	Ratio between measured and actual rest tumor volume	*0.64*	L	(18)

Parameter	Definition	*Value*	Unit	Source
$\mathbf{V_{tot,\ pro}}$	Total volume of the prostate	$\frac{0.016*BW}{71}$	L	(18)
$\mathbf{V_{tot,\ kid}}$	Total kidney volume	*0.3*	L	(38)
$\mathbf{V_{tot,\ li}}$	Total liver volume	*(0.023 * BW)*	L	(39)
$\mathbf{V_{tot,\ spl}}$	Total splenic volume	*(0.003 * BW)*	L	(39)
$\mathbf{V_{tot,\ GI}}$	Total volume of the GI-tract	$\frac{(0.385 + 0.548 + 0.104 + 0.15) * BW}{71}$	L	(18)
$\mathbf{V_{tot,\ par}}$	Total volume of the parotid glands	*0.032*	L	(40)
$\mathbf{V_{tot,\ sm}}$	Total volume of the submandibular glands	*0.0095*	L	(40)
$\mathbf{V_{tot,\ lg}}$	Total volume of the lacrimal glands	*0.00068*	L	(41)
$\mathbf{V_{tot,\ rm}}$	Total volume of the red marrow	$\frac{1.1*BW}{71}$	L	(18)
$\mathbf{V_{tot,\ mu}}$	Total volume of the muscles	$\frac{30.078 * BW}{71}$	L	(18)
$\mathbf{V_{tot,\ sk}}$	Total volume of the skin	$\frac{3.408 * BW}{71}$	L	(18)
$\mathbf{V_{tot,\ br}}$	Total volume of the brain	$\frac{1.45 * BW}{71}$	L	(18)
$\mathbf{V_{tot,\ ad}}$	Total adipose tissue volume	$\frac{13.465 * BW}{71}$	L	(18)
$\mathbf{V_{tot,\ hrt}}$	Total heart volume	$\frac{0.341 * BW}{71}$	L	(18)
$\mathbf{V_{tot,\ bo}}$	Total bone volume (without the red marrow)	$\frac{10.165 * BW}{71} - V_{tot,\ rm}$	L	(18)
$\mathbf{V_{tot,\ rest}}$	Total rest volume	$V_{tot,\ BW} - \sum_i V_{tot,\ i}$	L	(18)
$\mathbf{Fra_{vasc,\ i}}$	Vascular volume fraction of tissue		Fraction	(18)
$\mathbf{Fra_{vasc,lu}}$	Vascular volume fraction of the lungs	*0.055*	Fraction	(42)
$\mathbf{Fra_{vasc,tu}}$	Vascular volume fraction of tumors 1,2 and rest	$0.05 * (1 - H)$	Fraction	(18)
$\mathbf{Fra_{vasc,\ kid}}$	Vascular volume fraction of the kidneys	*0.055*	Fraction	(18)
$\mathbf{Fra_{vasc,\ li}}$	Vascular volume fraction of the liver	*0.085*	Fraction	(18)

Parameter	Definition	*Value*	Unit	Source
$Fra_{vasc,\ spl}$	Vascular volume fraction of the spleen	*0.12*	Fraction	(18)
$V_{ser,\ body}$	Serum volume of body	$2.8 * (1 - H) * BSA$	L	(18)
$V_{ser,\ ven}$	Venous serum volume	$(0.18 * V_{ser,body}) + (0.045 * V_{ser,body})$	L	(18)
$V_{ser,\ art}$	Arterial serum volume	$(0.06 * V_{ser,body}) + (0.045 * V_{ser,body})$	L	(18)
$V_{vasc,\ i}$	Vascular serum volume of tissue (i)		L	(18)
$V_{vasc,\ lu}$	Vascular lung volume	$V_{tot,lu} * Fra_{vasc,\ lu}$	L	(42)
$V_{vasc,\ tu1}$	Vascular volume of tumor 1	$V_{tot,tu1} * Fra_{vasc,tu}$	L	(18)
$V_{vasc,\ tu2}$	Vascular volume of tumor 2	$V_{tot,tu2} * Fra_{vasc,tu}$	L	(18)
$V_{vasc,\ turest}$	Vascular volume of the rest tumor	$V_{tot,turest} * Fra_{vasc,tu}$	L	(18)
$V_{vasc,\ pro}$	Vascular prostate volume	$0.004 * (1 - H) * V_{tot,pro}$	L	(18)
$V_{vasc,\ kid}$	Vascular kidney volume	$V_{tot,kid} * F_{vasc,kid}$	L	(18)
$V_{vasc,\ li}$	Vascular liver volume	$V_{tot,li} * F_{vasc,li}$	L	(18)
$V_{vasc,\ spl}$	Vascular spleen volume	$V_{tot,spl} * F_{vasc,spl}$	L	(18)
$V_{vasc,\ gi}$	Vascular volume of the GI-tract	$0.076 * V_{ser,body}$	L	(18)
$V_{vasc,\ par}$	Vascular parotid gland volume	$0.03 * (1 - H) * V_{tot,par}$	L	(18)
$V_{vasc,\ sm}$	Vascular submandibular gland volume	$0.03 * (1 - H) * V_{tot,sm}$	L	(18)
$V_{vasc,\ lg}$	Vascular lacrimal gland volume	$0.03 * (1 - H) * V_{tot,lg}$	L	(18)
$V_{vasc,\ rm}$	Vascular red marrow volume	$0.04 * V_{ser,body}$	L	(18)
$V_{vasc,\ mu}$	Vascular muscle volume	$0.14 * V_{ser,body}$	L	(18)
$V_{vasc,\ sk}$	Vascular skin volume	$0.03 * V_{ser,body}$	L	(18)
$V_{vasc,\ br}$	Vascular brain volume	$0.012 * V_{ser,body}$	L	(18)
$V_{vasc,\ ad}$	Vascular adipose tissue volume	$0.05 * V_{ser,body}$	L	(18)
$V_{vasc,\ hrt}$	Vascular heart volume	$0.01 * V_{ser,body}$	L	(18)

Parameter	Definition	*Value*	Unit	Source
$\mathbf{V}_{vasc,\ bo}$	Vascular bone volume (without the red marrow)	$(0.07 * V_{ser,body}) - V_{vasc,rm}$	L	(18)
$\mathbf{V}_{vasc,\ rest}$	Vascular rest volume	$V_{ser,body} - \sum_i V_{vasc,\ i}$	L	(18)
$\mathbf{Fra}_{int,\ i}$	Interstitial volume fraction of tissue (i)		Fraction	(18)
$\mathbf{Fra}_{int,\ lu}$	Interstitial volume fraction of the lungs	*0.3*	Fraction	(42)
$\mathbf{Fra}_{int,\ tu}$	Interstitial volume fraction of tumors 1, 2 and rest	*0.38*	Fraction	(18)
$\mathbf{Fra}_{int,\ kid}$	Interstitial volume fraction of the kidneys	*0.15*	Fraction	(18)
$\mathbf{Fra}_{int,\ li}$	Interstitial volume fraction of the liver	*0.2*	Fraction	(18)
$\mathbf{Fra}_{int,\ spl}$	Interstitial volume fraction of the spleen	*0.2*	Fraction	(18)
$\mathbf{Fra}_{int,\ gi}$	Interstitial volume fraction of the GI-tract	*0.1739634*	Fraction	(42)
$\mathbf{Fra}_{int,\ rest}$	Interstitial volume fraction of the rest tissue	*0.1712696*	Fraction	(42)
$\boldsymbol{\alpha}_i$	Ratio of interstitial to vascular volume		Fraction	(18)
$\boldsymbol{\alpha}_{rm}$	Ratio of interstitial to vascular volume of the red marrow	*3.7*	Fraction	(18)
$\boldsymbol{\alpha}_{mu}$	Ratio of interstitial to vascular volume of the muscles	*5.9*	Fraction	(18)
$\boldsymbol{\alpha}_{sk}$	Ratio of interstitial to vascular volume of the skin	*8.9*	Fraction	(18)
$\boldsymbol{\alpha}_{ad}$	Ratio of interstitial to vascular volume of the adipose tissue	*15.5*	Fraction	(18)
$\boldsymbol{\alpha}_{hrt}$	Ratio of interstitial to vascular volume of the heart	*3.7*	Fraction	(18)

Parameter	Definition	*Value*	Unit	Source
α_{bo}	Ratio of interstitial to vascular volume of the bones (without red marrow)	*8.4*	Fraction	(18)
$V_{int,\ i}$	Interstitial volume of tissue (i)		L	(18)
$V_{int,\ lu}$	Interstitial lung volume	$V_{tot,lu} * Fra_{int,lu}$	L	(18)
$V_{int,\ tu1}$	Interstitial volume of tumor 1	$V_{tot,tu1} * Fra_{int,tu1}$	L	(18)
$V_{int,\ tu2}$	Interstitial volume of tumor 2	$V_{\ tot,tu2} * Fra_{int,tu}$	L	(18)
$V_{int,\ turest}$	Interstitial volume of the rest tumor	$V_{tot,turest} * Fra_{int,tu}$	L	(18)
$V_{int,\ pro}$	Interstitial prostate volume	$0.25 * V_{tot,pro}$	L	(18)
$V_{int,\ kid}$	Interstitial kidney volume	$V_{tot,kid} * Fra_{int,kid}$	L	(18)
$V_{int,\ li}$	Interstitial liver volume	$V_{\ tot,li} * Fra_{int,li}$	L	(18)
$V_{int,\ spl}$	Interstititial spleen volume	$V_{\ tot,spl} * Fra_{int,spl}$	L	(18)
$V_{int,\ GI}$	Interstitial volume of the GI-tract	$V_{tot,gi} * Fra_{int,gi}$	L	(18)
$V_{int,\ par}$	Interstitial parotid gland volume	$0.23 * V_{tot,par}$	L	(18)
$V_{int,\ sm}$	Interstitial submandibular gland volume	$0.23 * V_{tot,sm}$	L	(18)
$V_{int,\ lg}$	Interstitial lacrimal gland volume	$0.23 * V_{tot,lg}$	L	(18)
$V_{int,\ rm}$	Interstitial red marrow volume	$V_{vasc,rm} * \alpha_{rm}$	L	(18)
$V_{int,\ mu}$	Interstitial muscle volume	$V_{vasc,mu} * \alpha_{mu}$	L	(18)
$V_{int,\ sk}$	Interstitial skin volume	$V_{vasc,sk} * \alpha_{sk}$	L	(18)
$V_{int,\ ad}$	Interstitial adipose tissue volume	$V_{vasc,ad} * \alpha_{ad}$	L	(18)
$V_{int,\ hrt}$	Interstitial heart volume	$V_{vasc,hrt} * \alpha_{hrt}$	L	(18)

Parameter	Definition	*Value*	Unit	Source
$\mathbf{V_{int,\,bo}}$	Interstitial bone bone volume (without red marrow)	$V_{vasc,bo} * \alpha_{bo}$	L	(18)
$\mathbf{V_{int,\,rest}}$	Interstitial rest tissue volume	$V_{tot,rest} * Fra_{int,rest}$	L	(18)
$\mathbf{F_{dens,\,i}}$	Flow density of tissue per unit mass (i)		$\frac{mL}{\min * g}$	(18)
$\mathbf{F_{dens,\,tu1}}$	Flow density of tumor 1	*0.1351538*	$\frac{mL}{\min * g}$	(18)
$\mathbf{F_{dens,\,tu2}}$	Flow density of tumor 2	*0.2676154*	$\frac{mL}{\min * g}$	(18)
$\mathbf{X_F}$	Ratio between actual and assumed flow density of the rest tumor	*0.53*	Fraction	(18)
$\mathbf{F_{dens,\,turest}}$	Flow density of the rest tumor	$X_F * \left(\frac{F_{dens,tu1} + F_{dens,tu2}}{2}\right)$	$\frac{mL}{\min * g}$	(18)
$\mathbf{F_{dens,\,pro}}$	Flow density of the prostate	$0.18 * (1 - H)$	$\frac{mL}{\min * g}$	(18)
$\mathbf{F_{dens,\,par}}$	Flow density of the parotid glands	*0.16*	$\frac{mL}{\min * g}$	(18)
$\mathbf{F_{dens,\,sm}}$	Flow density of the submandibular glands	$F_{dens,par}$	$\frac{mL}{\min * g}$	(18)
$\mathbf{F_{dens,\,lg}}$	Flow density of the lacrimal glands	$F_{dens,par}$	$\frac{mL}{\min * g}$	(18)
$\mathbf{F_{k,\,c}}$	Age-independent blood flow to kidney	*4.3*	$\frac{mL}{\min * g}$	(18)
$\mathbf{F_{k,\,age}}$	Age dependent blood flow to kidney	$F_{k,C} - (0.026 * Age)$	$\frac{mL}{\min * g}$	(18)
$\mathbf{F_{tot}}$	Total body flow	$V_{ser,body} * 1.23$	$\frac{L}{min}$	(18)
$\mathbf{F_i}$	Blood flow to tissue (i)		$\frac{L}{min}$	(18)
$\mathbf{F_{lu}}$	Lung flow	F_{tot}	$\frac{L}{min}$	(18)
$\mathbf{F_{tu1}}$	Flow to tumor 1	$F_{dens,tu1} * V_{tot,tu1}$	$\frac{L}{min}$	(18)
$\mathbf{F_{tu2}}$	Flow to tumor 2	$F_{dens,tu2} * V_{tot,tu2}$	$\frac{L}{min}$	(18)
$\mathbf{F_{turest}}$	Flow to the rest tumor	$F_{dens,pro} * V_{tot,turest}$	$\frac{L}{min}$	(18)
$\mathbf{F_{pro}}$	Prostate flow	$F_{dens,pro} * V_{tot,pro}$	$\frac{L}{min}$	(18)
$\mathbf{F_{kid}}$	Kidney flow	$F_{k,age} * V_{tot,kid} * (1 - H)$	$\frac{L}{min}$	(18)

Parameter	Definition	*Value*	Unit	Source
F_{li}	Liver flow	$0.065 * F_{tot}$	$\frac{L}{min}$	(18)
F_{spl}	Spleen flow	$0.03 * F_{tot}$	$\frac{L}{min}$	(18)
F_{GI}	Flow to the GI-tract	$0.16 * F_{tot}$	$\frac{L}{min}$	(18)
F_{par}	Parotid gland flow	$F_{dens,par} * V_{tot,par}$	$\frac{L}{min}$	(18)
F_{sm}	Submandibular gland flow	$F_{dens,sm} * V_{tot,sm}$	$\frac{L}{min}$	(18)
F_{lg}	Lacrimal gland flow	$F_{dens,lg} * V_{tot,lg}$	$\frac{L}{min}$	(18)
F_{rm}	Red marrow flow	$0.03 * F_{tot}$	$\frac{L}{min}$	(18)
F_{mu}	Muscle flow	$0.17 * F_{tot}$	$\frac{L}{min}$	(18)
F_{sk}	Skin flow	$0.05 * F_{tot}$	$\frac{L}{min}$	(18)
F_{br}	Brain flow	$0.12 * F_{tot}$	$\frac{L}{min}$	(18)
F_{ad}	Adipose tissue flow	$0.05 * F_{tot}$	$\frac{L}{min}$	(18)
F_{hrt}	Heart flow	$0.04 * F_{tot}$	$\frac{L}{min}$	(18)
F_{bo}	Bone flow (without red marrow)	$0.05 * F_{tot}$	$\frac{L}{min}$	(18)
F_{rest}	Flow to the rest tissue	$F_{tot} - \sum_i F_i$	$\frac{L}{min}$	(18)
Φ_{kid}	Ratio of sieving coefficients	*1*	Fraction	(29)
F_{fil}	Filtration flow of kidney	$\mathrm{eGFR} * \Phi\mathrm{kid}$	$\frac{L}{min}$	(18)
Fra_{ex}	Filtrated fraction of eGFR	*1*	Fraction	(24, 26)
F_{ex}	Excretion flow of kidneys	$F_{fil} * Fra_{ex}$	$\frac{L}{min}$	(18)
Ki	Permeability surface area product per unit mass		$\frac{mL}{\mathrm{min}*g}$	(18)
K_{mu}	Permeability surface area product of muscles per unit mass	*0.02*	$\frac{mL}{\mathrm{min}*g}$	(18)
K_{lu}	Permeability surface area product of lungs per unit mass	$K_{mu} * 100$	$\frac{mL}{\mathrm{min}*g}$	(18)
K_{tu}	Permeability surface area product of the tumors per unit mass	*0.6*	$\frac{mL}{\mathrm{min}*g}$	(18)

Parameter	Definition	*Value*	Unit	Source
K_{pro}	Permeability surface area product of the prostate per unit mass	*0.1*	$\frac{mL}{\min * g}$	(18)
K_{li}	Permeability surface area product of the liver per unit mass	$K_{mu} * 100$	$\frac{mL}{\min * g}$	(18)
K_{spl}	Permeability surface area product of the spleen per unit mass	K_{li}	$\frac{mL}{\min * g}$	(18)
K_{gi}	Permeability surface area product of the GI-tract per unit mass	*0.02*	$\frac{mL}{\min * g}$	(18)
K_{par}	Permeability surface area product of the parotid glands per unit mass	*0.4*	$\frac{mL}{\min * g}$	(18)
K_{sm}	Permeability surface area product of the submandibular glands per unit mass	K_{par}	$\frac{mL}{\min * g}$	(18)
K_{lg}	Permeability surface area product of the lacrimal glands per unit mass	K_{par}	$\frac{mL}{\min * g}$	(18)
K_{rm}	Permeability surface area product of the red marrow per unit mass	K_{li}	$\frac{mL}{\min * g}$	(18)
K_{sk}	Permeability surface area product of the skin per unit mass	*0.02*	$\frac{mL}{\min * g}$	(18)
K_{ad}	Permeability surface area product of the adipose tissue per unit mass	*0.02*	$\frac{mL}{\min * g}$	(18)
K_{hrt}	Permeability surface area product of the heart per unit mass	*0.02*	$\frac{mL}{\min * g}$	(18)
K_{bo}	Permeability surface area product of the bones per unit mass	*0.02*	$\frac{mL}{\min * g}$	(18)

Parameter	Definition	*Value*	Unit	Source
K_{pro}	Permeability surface area product of the prostate per unit mass	*0.02*	$\frac{mL}{\min * g}$	(18)
PS_{lu}	Permeability surface area product of the lungs	$K_{lu} * V_{tot,lu}$	$\frac{mL}{min}$	(18)
PS_{tu1}	Permeability surface area product of tumor 1	$K_{tu} * V_{tot,tu1}$	$\frac{mL}{min}$	(18)
PS_{tu2}	Permeability surface area product of tumor 2	$K_{tu} * V_{tot,tu2}$	$\frac{mL}{min}$	(18)
PS_{turest}	Permeability surface area product of the rest tumor	$K_{tu} * V_{tot,turest}$	$\frac{mL}{min}$	(18)
PS_{pro}	Permeability surface area product of the prostate	$K_{pro} * V_{tot,pro}$	$\frac{mL}{min}$	(18)
PS_{li}	Permeability surface area product of the liver	$K_{li} * V_{tot,li}$	$\frac{mL}{min}$	(18)
PS_{spl}	Permeability surface area product of the spleen	$K_{spl} * V_{tot,spl}$	$\frac{mL}{min}$	(18)
PS_{gi}	Permeability surface area product of the GI-tract	$K_{gi} * V_{tot,gi}$	$\frac{mL}{min}$	(18)
PS_{par}	Permeability surface area product of the parotid glands	$K_{par} * V_{tot,par}$	$\frac{mL}{min}$	(18)
PS_{sm}	Permeability surface area product of the submandibular glands	$K_{sm} * V_{tot,sm}$	$\frac{mL}{min}$	(18)
PS_{lg}	Permeability surface area product of the lacrimal glands	$K_{lg} * V_{tot,lg}$	$\frac{mL}{min}$	(18)
PS_{rm}	Permeability surface area product of the red marrow	$K_{rm} * V_{tot,rm}$	$\frac{mL}{min}$	(18)
PS_{mu}	Permeability surface area product of the muscles	$K_{mu} * V_{tot,mu}$	$\frac{mL}{min}$	(18)

Parameter	Definition	*Value*	Unit	Source
PS_{sk}	Permeability surface area product of the skin	$K_{sk} * V_{tot,sk}$	$\frac{mL}{min}$	(18)
PS_{ad}	Permeability surface area product of the adipose tissue	$K_{ad} * V_{tot,ad}$	$\frac{mL}{min}$	(18)
PS_{hrt}	Permeability surface area product of the heart	$K_{thrt} * V_{tot,hrt}$	$\frac{mL}{min}$	(18)
PS_{bo}	Permeability surface area product of the bnes	$K_{bo} * V_{tot,bo}$	$\frac{mL}{min}$	(18)
PS_{rest}	Permeability surface area product of the rest tissue	$K_{rest} * V_{tot,rest}$	$\frac{mL}{min}$	(18)
$Labda_{int,\ tu}$	Internalisation rate of 18F-DCFPyL by the tumors	*0.001*	Min^{-1}	(18)
$Labda_{int,\ turest}$	Internalisation rate of 18F-DCFPyL by the rest tumor	*0.001*	Min^{-1}	(18)
$Labda_{int,\ nt}$	Internalisation rate of 18F-DCFPyL by normal tissue	$Labda_{int,\ tu}$	Min^{-1}	(18)
$Labda_{int,\ pro}$	Internalisation rate of 18F-DCFPyL by the prostate	$Labda_{int,\ tu}$	Min^{-1}	(18)
$Labda_{int,\ kid}$	Internalisation rate of 18F-DCFPyL by the kidneys	$Labda_{int,\ tu}$	Min^{-1}	(18)
$Labda_{int,\ li}$	Internalisation rate of 18F-DCFPyL by the liver	$Labda_{int,\ tu}$	Min^{-1}	(18)
$Labda_{int,\ spl}$	Internalisation rate of 18F-DCFPyL by the spleen	$Labda_{int,\ tu}$	Min^{-1}	(18)
$Labda_{int,\ gi}$	Internalisation rate of 18F-DCFPyL by the GI-tract	$Labda_{int,\ tu}$	Min^{-1}	(18)
$Labda_{int,\ par}$	Internalisation rate of 18F-DCFPyL by the parotid glands	$Labda_{int,\ tu}$	Min^{-1}	(18)

Parameter	Definition	*Value*	Unit	Source
$Labda_{int, sm}$	Internalisation rate of 18F-DCFPyL by the submandibular glands	$Labda_{int, tu}$	Min^{-1}	(18)
$Labda_{int, lg}$	Internalisation rate of 18F-DCFPyL by the lacrimal glands	$Labda_{int, tu}$	Min^{-1}	(18)
$Labda_{rel, tu}$	Release and degradation rate of 18F-DCFPyL by the tumors	*1.4e-4*	Min^{-1}	(18)
$Labda_{rel, turest}$	Release and degradation rate of 18F-DCFPyL by the rest tumor	$Labda_{rel, tu}$	Min^{-1}	(18)
$Labda_{rel, kid}$	Release and degradation rate of 18F-DCFPyL by the kidneys	*2.3e-4*	Min^{-1}	(18)
$Labda_{rel, nt}$	Release and degradation rate of 18F-DCFPyL by normal tissue	$Labda_{rel, kid}$	Min^{-1}	(18)
$Labda_{rel, pro}$	Release and degradation rate of 18F-DCFPyL by the prostate	$Labda_{rel, nt}$	Min^{-1}	(18)
$Labda_{rel, li}$	Release and degradation rate of 18F-DCFPyL by the liver	$Labda_{rel, kid}$	Min^{-1}	(18)
$Labda_{rel, spl}$	Release and degradation rate of 18F-DCFPyL by the spleen	$Labda_{rel, kid}$	Min^{-1}	(18)
$Labda_{rel, gi}$	Release and degradation rate of 18F-DCFPyL by the GI-tract	$Labda_{rel, nt}$	Min^{-1}	(18)
$Labda_{rel, par}$	Release and degradation rate of 18F-DCFPyL by the parotid glands	*0.00037*	Min^{-1}	(18)

Parameter	Definition	*Value*	Unit	Source
$Labda_{rel, sm}$	Release and degradation rate of 18F-DCFPyL by the submandibular glands	$Labda_{rel, par}$	Min^{-1}	(18)
$Labda_{rel, lg}$	Release and degradation rate of 18F-DCFPyL by the lacrimal glands	$Labda_{rel, par}$	Min^{-1}	(18)
$R_{dens, tu1}$	PSMA receptor density of tumor 1	*44.93846*	$\frac{Nmol}{L}$	(18)
$R_{dens, tu2}$	PSMA receptor density of tumor 2	*47.38462*	$\frac{Nmol}{L}$	(18)
X_R	Ratio between assumed receptor density and actual receptor density of the rest tumor	1.4	*Fraction*	(18)
$R_{dens, turest}$	PSMA receptor density of the rest tumor	$X_R \frac{R_{dens.tu1} + R_{dens.tu2}}{2}$	$\frac{Nmol}{L}$	(18)
$R_{dens, kid}$	PSMA receptor density of the kidneys	*18*	$\frac{Nmol}{L}$	(18)
$R_{dens, pro}$	PSMA receptor density of the prostate	$R_{dens,turest} * 0.1$	$\frac{Nmol}{L}$	(18)
$R_{dens, li}$	PSMA receptor density of the liver	$R_{dens,pro} * 0.05$	$\frac{Nmol}{L}$	(18)
$R_{dens, spl}$	PSMA receptor density of the spleen	$R_{dens,kid} * 0.2$	$\frac{Nmol}{L}$	(18)
$R_{dens, gi}$	PSMA receptor density of the GI-tract	$R_{dens,pro} * 0.06$	$\frac{Nmol}{L}$	(18)
$R_{dens, par}$	PSMA receptor density of the parotid glands	*42*	$\frac{Nmol}{L}$	(18)
$R_{dens, sm}$	PSMA receptor density of the submandibular glands	$R_{dens, par}$	$\frac{Nmol}{L}$	(18)
$R_{dens, lg}$	PSMA receptor density of the lacrimal glands	$R_{dens, par}$	$\frac{Nmol}{L}$	(18)
$R_{tot, tu1}$	Total PSMA receptor number of tumor 1	$R_{dens,tu1} * V_{tot,tu1}$	Nmol	(18)
$R_{tot, tu2}$	Total PSMA receptor number of tumor 2	$R_{dens,tu2} * V_{tot,tu2}$	Nmol	(18)

Parameter	Definition	*Value*	Unit	Source
$\mathbf{R_{tot,\ turest}}$	Total PSMA receptor number of the rest tumor	$R_{dens,turest} * V_{tot,turest}$	Nmol	(18)
$\mathbf{R_{tot,\ pro}}$	Total PSMA receptor number of the prostate	$R_{dens,pro} * V_{tot,pro}$	Nmol	(18)
$\mathbf{R_{tot,\ kid}}$	Total PSMA receptor number of the kidneys	$R_{dens,kid} * V_{tot,kid}$	Nmol	(18)
$\mathbf{R_{tot,\ li}}$	Total PSMA receptor number of the liver	$R_{dens,li} * V_{tot,li}$	Nmol	(18)
$\mathbf{R_{tot,\ spl}}$	Total PSMA receptor number of the spleen	$R_{dens,spl} * V_{tot,spl}$	Nmol	(18)
$\mathbf{R_{tot,\ gi}}$	Total PSMA receptor number of the GI-tract	$R_{dens,gi} * V_{tot,gi}$	Nmol	(18)
$\mathbf{R_{tot,\ par}}$	Total PSMA receptor number of the parotid glands	$R_{dens,par} * V_{tot,par}$	Nmol	(18)
$\mathbf{R_{tot,\ sm}}$	Total PSMA receptor number of submandibular glands	$R_{dens,sm} * V_{tot,sm}$	Nmol	(18)
$\mathbf{R_{tot,\ lg}}$	Total PSMA receptor number of the lacrimal glands	$R_{dens,lg} * V_{tot,lg}$	Nmol	(18)
$\mathbf{A_{vasc,\ i}}$	Free vascular ligand in tissue (i)	*Simulated*	nmol	(18)
$\mathbf{A_{int,\ i}}$	Free interstitial ligand in tissue (i)	*Simulated*	nmol	(18)
$\mathbf{AR_i}$	Ligand bound to receptor on cell surface of tissue (i)	*Simulated*	nmol	(18)
$\mathbf{A_{intern,\ i}}$	Free internalized ligand in in tissue (i)	*Simulated*	nmol	(18)
$\mathbf{A_{lum,kid}}$	Free ligand in the kidney lumen	*Simulated*	nmol	(18)
$\mathbf{RF_i}$	Unbound receptors in the PSMA-positive tissues i)	*Simulated*	Nmol	(27)

MODEL VALIDATION

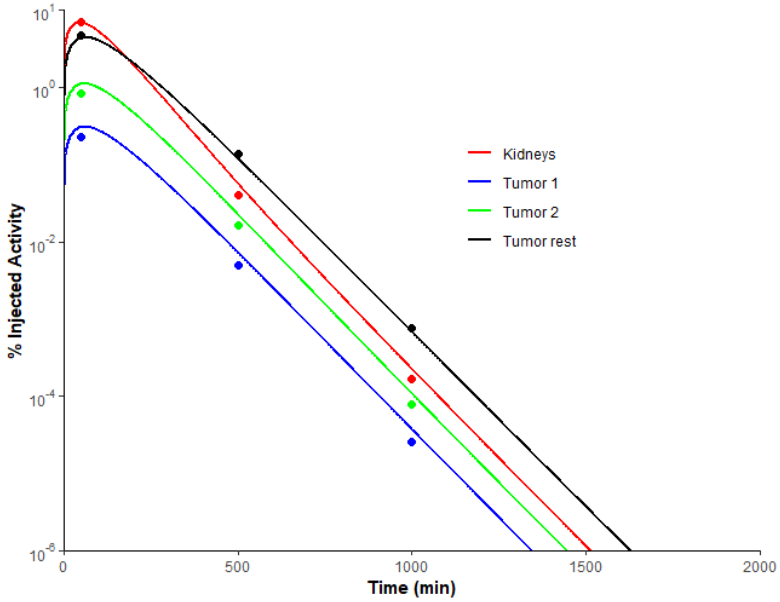

Supplemental figure 2. The simulation of patient 4 as reported by Begum *et al*. The solid lines are predictions made by our model and the dots are values reported by Begum *et al*.

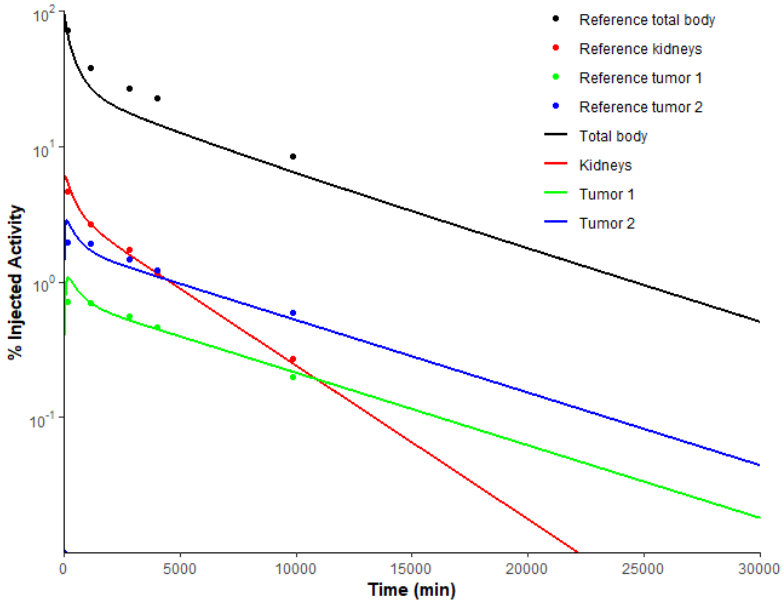

Supplemental figure 3. The simulation of patient 4 as reported by Begum *et al*. The solid lines are predictions made by our model and the dots are observations reported by Begum *et al*.

INDIVIDUAL PATIENT SIMULATIONS

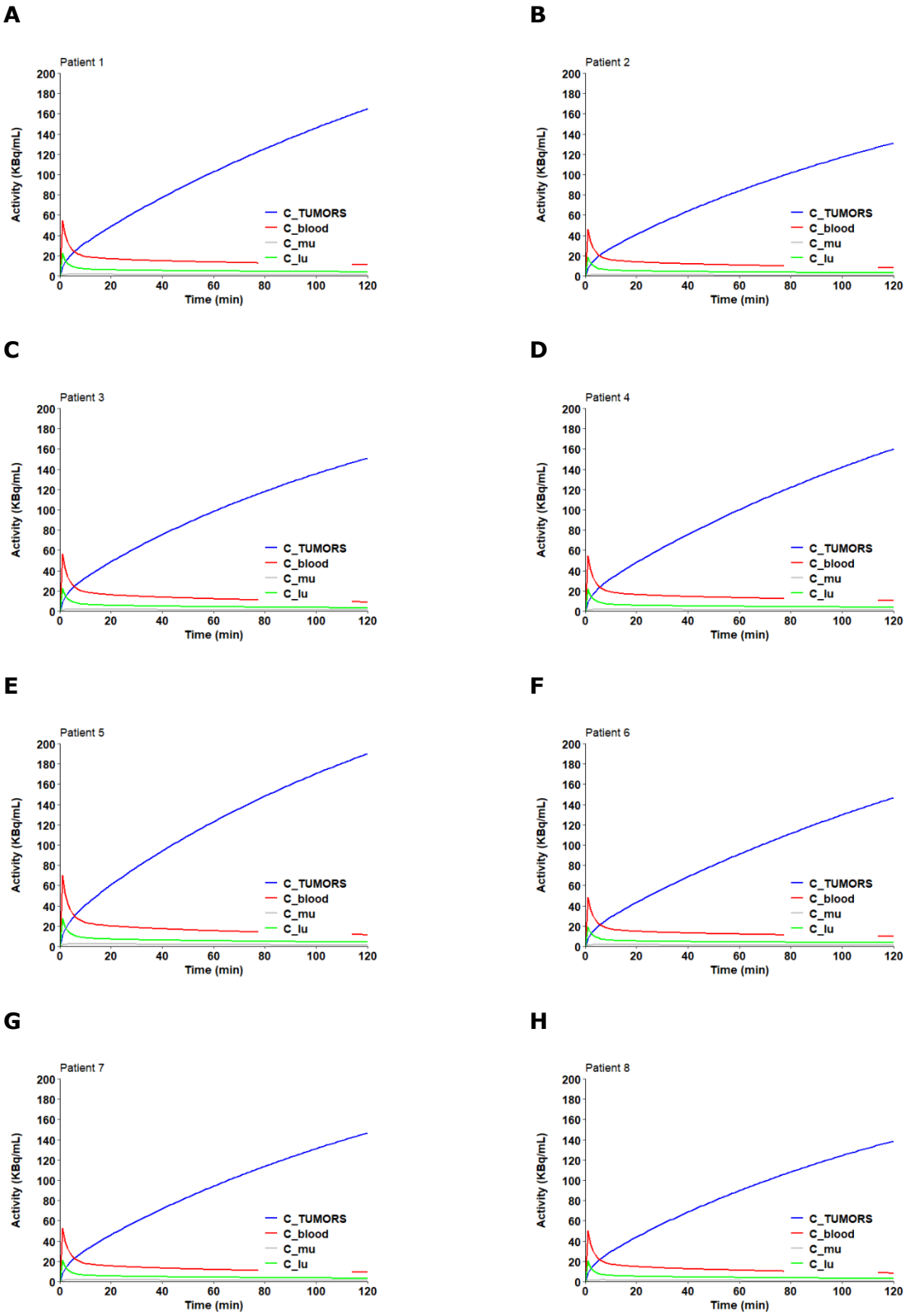

Supplemental figure 4. The individual simulations of the patient population included by Janssen *et al*. (26)

SENSITIVITEITS ANALYSIS

PARAMETER VALUES

Supplemental table 2. The sensitivity analysis parameters.

Parameter	Baseline value (lower value, upper value)	Source
BW (kg)	92 (64, 119)	(26, 30)
BH (cm)	181 (171, 191)	(26, 30)
Age (y)	68 (56, 81)	(26, 30)
eGFR (mL/min)	75 (15, 30, 45, 60, 90, 120)	(43)
Hematocrit (Ratio)	0.45 (0.27, 0.55)	(26, 44)
Total tumor burden (TTV) (L) **Tumor 1** **Tumor 2** **Tumor rest**	0.0214 (0.0106 – 0.0632) 0.02313625 * TTV **(A)** 0.02956298 * TTV **(A)** 0.9473008 * TTV **(A)**	(18, 30)
X_V	0.64 (0.12, 1.16)	(18)
Kidney volume (L)	0.3 (0.22, 0.380)	(38)
Liver volume (L)	1.8 (1.020, 2.190)	(45)
Spleen volume (L)	0.180 (0.074, 0.229)	(45)
Parotid glands volume (L)	0.032 (0.028792, 0.035082)	(40)
Submandibular glands volume (L)	0.0095 (0.00831, 0.01051)	(40)
Lacrimal glands volume (L)	0.00068 (0.000198, 0.001162)	(41)
Dose activity (GBq)	0.3 (0.292, 0.314)	(26)
Specific activity (GBq/nanomoles)	0.045 (0.0162, 0.0785)	In house measurements **(B)**
F_dens_tu1	0.1351538 (0.037, 0.3658439) **(C)**	(18)
F_dens_tu2	0.2676154 (0.045, 1.177352) **(C)**	(18)

Parameter	Baseline value (lower value, upper value)	Source
X_F	0.53 (0.52986, 0.53014)	(18)
F_k_age_c	4.3 (3, 5.6)	(18)
R_dens_tu1	44.93846 (0, 98.68413) **(D)**	(18)
R_dens_tu2	47.38462 (0, 106.6329) **(D)**	(18)
X_R	1.4 (0, 2.8) **(E)**	(18)
R_dens_kid	18 (12.2, 23.8)	(18)
Labda_rel_tu	$1.4e^{-4}$ ($2.6e^{-5}$, $2.54e^{-4}$)	(18)
Labda_rel_kid	$2.3e^{-4}$ ($1.12e^{-4}$, $3.48e^{-4}$)	(18)

Notes
Ranges were taken from literature. Upper and lower limits were either directly taken from literature data or calculated using two times the standard deviation.
A. Based on ratio of tumor volumes between tumors as reported by Begum *et al*. (18)
B. Averages were based on in house measurements reports on specific activity of 18F-DCFPYL administrations.
C. Averages were taken from literature data. The upper limit was based on two times the standard deviation. The lower limit was taken from the lowest reported value, because otherwise the flow density would become a negative value.
D. Averages were taken from literature data. The upper limit was based on two times the standard deviation. The lower limit was fixed on zero as negative receptor densities are not possible.
E. No standard deviation was reported for the X_R value in literature. A range was used between 0 and twice the baseline value.

SENSITIVITY ANALYSIS RESULTS

A

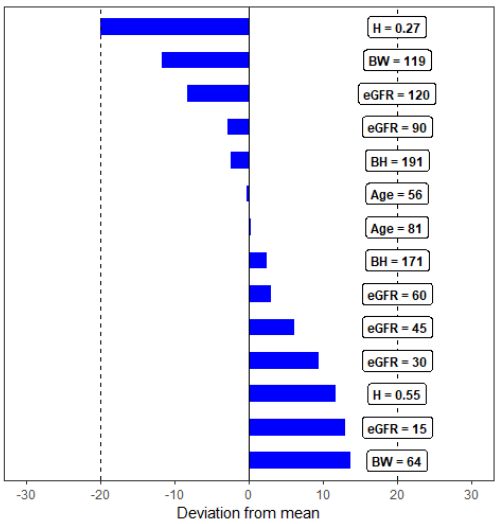

B

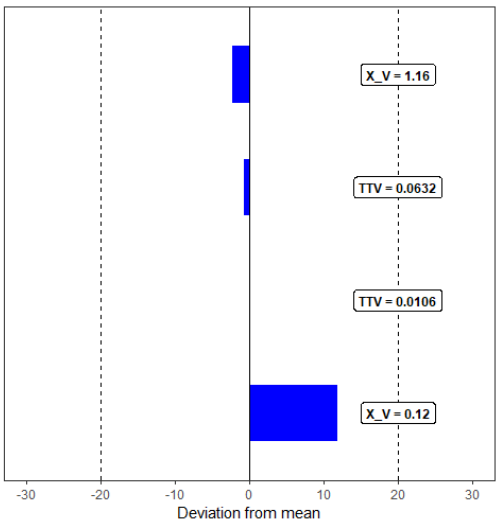

C

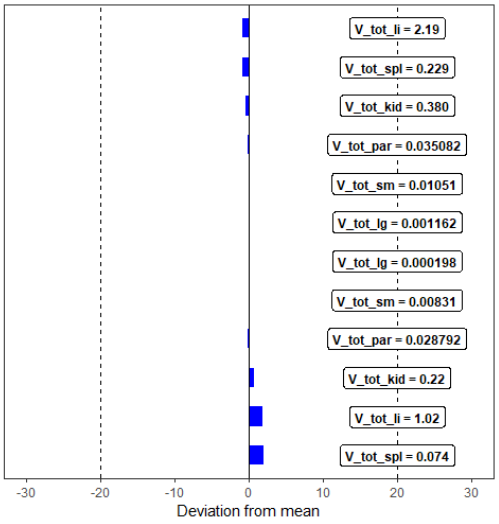

D

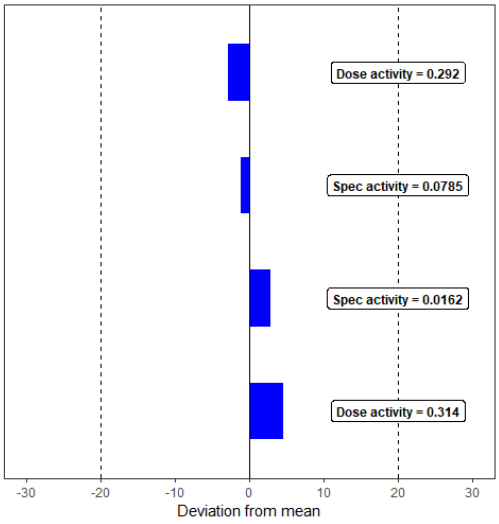

E

F

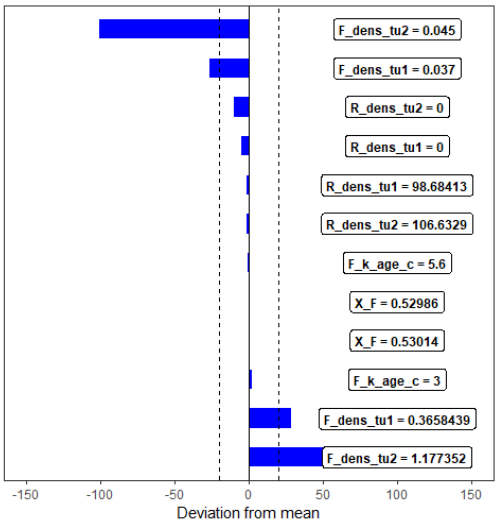

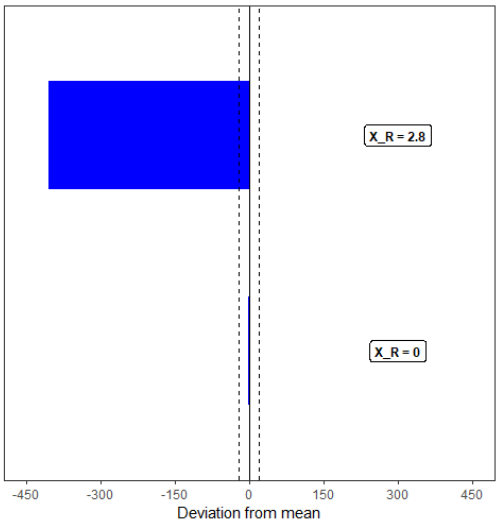

G

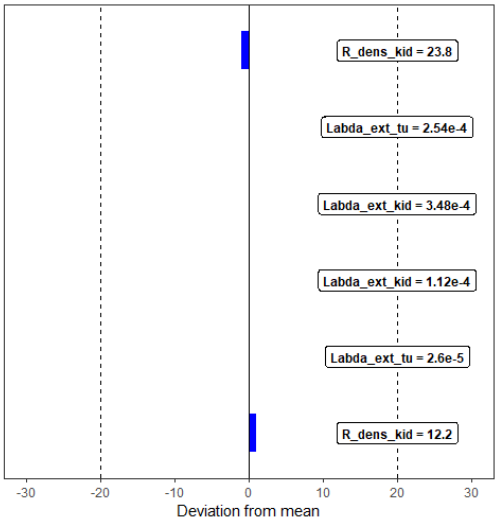

Supplemental figure 5. Waterfall plots of the sensitivity analysis.

MODEL SCRIPT

```
# ODE Model
PBPK_Model_DCFPYLF18 <- function(t, state, parameters){
  with(as.list(c(state, parameters)),{
    #
    # Veins
    dA_ven           <- (
                      + (F_kid * (A_vasc_kid/V_vasc_kid))
                      + (F_tu1 * (A_vasc_tu1/V_vasc_tu1))
                      + (F_tu2 * (A_vasc_tu2/V_vasc_tu2))
                      + (F_turest * (A_vasc_turest/V_vasc_turest))
                      + (F_pro * (A_vasc_pro/V_vasc_pro))
                      + ((F_li + F_spl + F_gi) * (A_vasc_li/V_vasc_li))
                      + (F_par * (A_vasc_par/V_vasc_par))
                      + (F_sm * (A_vasc_sm/V_vasc_sm))
                      + (F_lg * (A_vasc_lg/V_vasc_lg))
                      + (F_rm * (A_vasc_rm/V_vasc_rm))
                      + (F_mu * (A_vasc_mu/V_vasc_mu))
                      + (F_sk * (A_vasc_sk/V_vasc_sk))
                      + (F_br * (A_vasc_br/V_vasc_br))
                      + (F_ad * (A_vasc_ad/V_vasc_ad))
                      + (F_hrt * (A_vasc_hrt/V_vasc_hrt))
                      + (F_bo * (A_vasc_bo/V_vasc_bo))
                      + (F_rest * (A_vasc_rest/V_vasc_rest))
                      - (F_lu * (A_ven/V_ser_ven))
                     )
    #
    # Arteries
    dA_art           <- ( + (F_lu/V_vasc_lu*A_vasc_lu)
                      - (F_kid * (A_art/V_ser_art))
                      - (F_tu1 * (A_art/V_ser_art))
                      - (F_tu2 * (A_art/V_ser_art))
                      - (F_turest * (A_art/V_ser_art))
                      - (F_pro * (A_art/V_ser_art))
                      - (F_li * (A_art/V_ser_art))
                      - (F_spl * (A_art/V_ser_art))
                      - (F_gi * (A_art/V_ser_art))
                      - (F_par * (A_art/V_ser_art))
                      - (F_sm * (A_art/V_ser_art))
                      - (F_lg * (A_art/V_ser_art))
                      - (F_rm * (A_art/V_ser_art))
                      - (F_mu * (A_art/V_ser_art))
                      - (F_sk * (A_art/V_ser_art))
                      - (F_br * (A_art/V_ser_art))
                      - (F_ad * (A_art/V_ser_art))
                      - (F_hrt * (A_art/V_ser_art))
                      - (F_bo * (A_art/V_ser_art))
                      - (F_rest * (A_art/V_ser_art))
                     )
    #
    # Lungs
    dA_vasc_lu        <- F_lu * (A_ven/V_ser_ven) - F_lu * (A_vasc_lu/V_vasc_lu) - PS_lu * (A_vasc_lu/V_vasc_lu) + PS_lu *
(A_int_lu/V_int_lu)
    dA_int_lu         <- PS_lu * (A_vasc_lu/V_vasc_lu) - PS_lu * (A_int_lu/V_int_lu)
    #
    # Kidneys
    dA_vasc_kid       <- F_kid * (A_art/V_ser_art) - F_kid * (A_vasc_kid/V_vasc_kid) - F_fil * (A_vasc_kid/V_vasc_kid)
    dA_int_kid        <- F_fil * (A_vasc_kid/V_vasc_kid) - F_ex * (A_int_kid/V_int_kid) - (k_on * A_int_kid * RF_kid/V_int_kid) + k_off * AR_kid
    dAR_kid           <- (k_on * A_int_kid * RF_kid/V_int_kid) - k_off * AR_kid - Labda_int_kid * AR_kid
    dA_intern_kid     <- Labda_int_kid * AR_kid - Labda_ext_kid * A_intern_kid
    #
    # Tumor 1
    dA_vasc_tu1       <- F_tu1 * (A_art/V_ser_art) - F_tu1 * (A_vasc_tu1/V_vasc_tu1) - PS_tu1 * (A_vasc_tu1/V_vasc_tu1) + PS_tu1 *
(A_int_tu1/V_int_tu1)
    dA_int_tu1        <- PS_tu1 * (A_vasc_tu1/V_vasc_tu1) - PS_tu1 * (A_int_tu1/V_int_tu1) - (k_on * A_int_tu1 * RF_tu1/V_int_tu1) + k_off *
AR_tu1
    dAR_tu1           <- (k_on * A_int_tu1 * RF_tu1/V_int_tu1) - k_off * AR_tu1 - Labda_int_tu * AR_tu1
    dA_intern_tu1     <- Labda_int_tu * AR_tu1 - Labda_ext_tu * A_intern_tu1
    #
    # Tumor 2
    dA_vasc_tu2       <- F_tu2 * (A_art/V_ser_art) - F_tu2 * (A_vasc_tu2/V_vasc_tu2) - PS_tu2 * (A_vasc_tu2/V_vasc_tu2) + PS_tu2 *
(A_int_tu2/V_int_tu2)
    dA_int_tu2        <- PS_tu2 * (A_vasc_tu2/V_vasc_tu2) - PS_tu2 * (A_int_tu2/V_int_tu2) - (k_on * A_int_tu2 * RF_tu2/V_int_tu2) + k_off *
AR_tu2
    dAR_tu2           <- (k_on * A_int_tu2 * RF_tu2/V_int_tu2) - k_off * AR_tu2 - Labda_int_tu * AR_tu2
    dA_intern_tu2     <- Labda_int_tu * AR_tu2 - Labda_ext_tu * A_intern_tu2
    #
    # Tumors rest
    dA_vasc_turest    <- F_turest * (A_art/V_ser_art) - F_turest * (A_vasc_turest/V_vasc_turest) - PS_turest * (A_vasc_turest/V_vasc_turest)
+ PS_turest * (A_int_turest/V_int_turest)
    dA_int_turest     <- PS_turest * (A_vasc_turest/V_vasc_turest) - PS_turest * (A_int_turest/V_int_turest) - (k_on * A_int_turest *
RF_turest/V_int_turest) + k_off * AR_turest
    dAR_turest        <- (k_on * A_int_turest * RF_turest/V_int_turest) - k_off * AR_turest - Labda_int_turest * AR_turest
    dA_intern_turest  <- Labda_int_turest * AR_turest - Labda_ext_turest * A_intern_turest
    #
    # Prostate
    dA_vasc_pro       <- F_pro * (A_art/V_ser_art) - F_pro * (A_vasc_pro/V_vasc_pro) - PS_pro * (A_vasc_pro/V_vasc_pro) + PS_pro *
(A_int_pro/V_int_pro)
    dA_int_pro        <- PS_pro * (A_vasc_pro/V_vasc_pro) - PS_pro * (A_int_pro/V_int_pro) - (k_on * A_int_pro * RF_pro/V_int_pro) +  k_off
* AR_pro
    dAR_pro           <- (k_on * A_int_pro * RF_pro/V_int_pro) - k_off * AR_pro - Labda_int_pro * AR_pro
    dA_intern_pro     <- Labda_int_pro * AR_pro - Labda_ext_pro * A_intern_pro
    #
```

```
    # Liver
    dA_vasc_li        <- F_li * (A_art/V_ser_art) - (F_li + F_spl + F_gi) * (A_vasc_li/V_vasc_li) + F_spl * (A_vasc_spl/V_vasc_spl) + F_gi *
(A_vasc_gi/V_vasc_gi) - PS_li * (A_vasc_li/V_vasc_li) + PS_li * (A_int_li/V_int_li)
    dA_int_li         <- PS_li * (A_vasc_li/V_vasc_li) - PS_li * (A_int_li/V_int_li) - (k_on * A_int_li * RF_li/V_int_li) + k_off * AR_li
    dAR_li            <- (k_on * A_int_li * RF_li/V_int_li) - k_off * AR_li - Labda_int_li * AR_li
    dA_intern_li      <- Labda_int_li * AR_li - Labda_ext_li * A_intern_li
    #
    # Spleen
    dA_vasc_spl       <- F_spl * (A_art/V_ser_art) - F_spl * (A_vasc_spl/V_vasc_spl) - PS_spl * (A_vasc_spl/V_vasc_spl) + PS_spl *
(A_int_spl/V_int_spl)
    dA_int_spl        <- PS_spl * (A_vasc_spl/V_vasc_spl) - PS_spl * (A_int_spl/V_int_spl) - (k_on * A_int_spl * RF_spl/V_int_spl) +  k_off *
AR_spl
    dAR_spl           <- (k_on * A_int_spl * RF_spl/V_int_spl) - k_off * AR_spl - Labda_int_spl * AR_spl
    dA_intern_spl     <- Labda_int_spl * AR_spl - Labda_ext_spl * A_intern_spl
    #
    # GI-Tract
    dA_vasc_gi        <- F_gi * (A_art/V_ser_art) - F_gi * (A_vasc_gi/V_vasc_gi) - PS_gi * (A_vasc_gi/V_vasc_gi) + PS_gi * (A_int_gi/V_int_gi)
    dA_int_gi         <- PS_gi * (A_vasc_gi/V_vasc_gi) - PS_gi * (A_int_gi/V_int_gi) - (k_on * A_int_gi * RF_gi/V_int_gi) + k_off * AR_gi
    dAR_gi            <- (k_on * A_int_gi * RF_gi/V_int_gi) - k_off * AR_gi - Labda_int_gi * AR_gi
    dA_intern_gi      <- Labda_int_gi * AR_gi - Labda_ext_gi * A_intern_gi
    #
    # Parotid glands
    dA_vasc_par       <- F_par * (A_art/V_ser_art) - F_par * (A_vasc_par/V_vasc_par) - PS_par * (A_vasc_par/V_vasc_par) + PS_par *
(A_int_par/V_int_par)
    dA_int_par        <- PS_par * (A_vasc_par/V_vasc_par) - PS_par * (A_int_par/V_int_par) - (k_on * A_int_par * RF_par/V_int_par) + k_off *
AR_par
    dAR_par           <- (k_on * A_int_par * RF_par/V_int_par) - k_off * AR_par - Labda_int_par * AR_par
    dA_intern_par     <- Labda_int_par * AR_par - Labda_ext_par * A_intern_par
    #
    # Submandibular glands
    dA_vasc_sm        <- F_sm * (A_art/V_ser_art) - F_sm * (A_vasc_sm/V_vasc_sm) - PS_sm * (A_vasc_sm/V_vasc_sm) + PS_sm *
(A_int_sm/V_int_sm)
    dA_int_sm         <- PS_sm * (A_vasc_sm/V_vasc_sm) - PS_sm * (A_int_sm/V_int_sm) - (k_on * A_int_sm * RF_sm/V_int_sm) + k_off *
AR_sm
    dAR_sm            <- (k_on * A_int_sm * RF_sm/V_int_sm) - k_off * AR_sm - Labda_int_sm * AR_sm
    dA_intern_sm      <- Labda_int_sm * AR_sm - Labda_ext_sm * A_intern_sm
    #
    # Lacrimal glands
    dA_vasc_lg        <- F_lg * (A_art/V_ser_art) - F_lg * (A_vasc_lg/V_vasc_lg) - PS_lg * (A_vasc_lg/V_vasc_lg) + PS_lg * (A_int_lg/V_int_lg)
    dA_int_lg         <- PS_lg * (A_vasc_lg/V_vasc_lg) - PS_lg * (A_int_lg/V_int_lg) - (k_on * A_int_lg * RF_lg/V_int_lg) + k_off * AR_lg
    dAR_lg            <- (k_on * A_int_lg * RF_lg/V_int_lg) - k_off * AR_lg - Labda_int_lg * AR_lg
    dA_intern_lg      <- Labda_int_lg * AR_lg - Labda_ext_lg * A_intern_lg
    #
    # Red marrow
    dA_vasc_rm        <- F_rm * (A_art/V_ser_art) - F_rm * (A_vasc_rm/V_vasc_rm) - PS_rm * (A_vasc_rm/V_vasc_rm) + PS_rm *
(A_int_rm/V_int_rm)
    dA_int_rm         <- PS_rm * (A_vasc_rm/V_vasc_rm) - PS_rm * (A_int_rm/V_int_rm)
    #
    # Muscles
    dA_vasc_mu        <- F_mu * (A_art/V_ser_art) - F_mu * (A_vasc_mu/V_vasc_mu) - PS_mu * (A_vasc_mu/V_vasc_mu) + PS_mu *
(A_int_mu/V_int_mu)
    dA_int_mu         <- PS_mu * (A_vasc_mu/V_vasc_mu) - PS_mu * (A_int_mu/V_int_mu)
    #
    # Skin
    dA_vasc_sk        <- F_sk * (A_art/V_ser_art) - F_sk * (A_vasc_sk/V_vasc_sk) - PS_sk * (A_vasc_sk/V_vasc_sk) + PS_sk *
(A_int_sk/V_int_sk)
    dA_int_sk         <- PS_sk * (A_vasc_sk/V_vasc_sk) - PS_sk * (A_int_sk/V_int_sk)
    #
    # Brains
    dA_vasc_br        <- F_br * (A_art/V_ser_art) - F_br * (A_vasc_br/V_vasc_br)
    #
    # Adipose tissue
    dA_vasc_ad        <- F_ad * (A_art/V_ser_art) - F_ad * (A_vasc_ad/V_vasc_ad) - PS_ad * (A_vasc_ad/V_vasc_ad) + PS_ad *
(A_int_ad/V_int_ad)
    dA_int_ad         <- PS_ad * (A_vasc_ad/V_vasc_ad) - PS_ad * (A_int_ad/V_int_ad)
    #
    # Heart
    dA_vasc_hrt       <- F_hrt * (A_art/V_ser_art) - F_hrt * (A_vasc_hrt/V_vasc_hrt) - PS_hrt * (A_vasc_hrt/V_vasc_hrt) + PS_hrt *
(A_int_hrt/V_int_hrt)
    dA_int_hrt        <- PS_hrt * (A_vasc_hrt/V_vasc_hrt) - PS_hrt * (A_int_hrt/V_int_hrt)
    #
    # Bone
    dA_vasc_bo        <- F_bo * (A_art/V_ser_art) - F_bo * (A_vasc_bo/V_vasc_bo) - PS_bo * (A_vasc_bo/V_vasc_bo) + PS_bo *
(A_int_bo/V_int_bo)
    dA_int_bo         <- PS_bo * (A_vasc_bo/V_vasc_bo) - PS_bo * (A_int_bo/V_int_bo)
    #
    # Rest
    dA_vasc_rest      <- F_rest * (A_art/V_ser_art) - F_rest * (A_vasc_rest/V_vasc_rest) - PS_rest * (A_vasc_rest/V_vasc_rest) + PS_rest *
(A_int_rest/V_int_rest)
    dA_int_rest       <- PS_rest * (A_vasc_rest/V_vasc_rest) - PS_rest * (A_int_rest/V_int_rest)
    #
    # Receptoren
    dRF_kid           <- k_off * AR_kid - (k_on * A_int_kid * RF_kid/V_int_kid) + Labda_int_kid * AR_kid
    dRF_tu1           <- k_off * AR_tu1 - (k_on * A_int_tu1 * RF_tu1/V_int_tu1) + Labda_int_tu * AR_tu1
    dRF_tu2           <- k_off * AR_tu2 - (k_on * A_int_tu2 * RF_tu2/V_int_tu2) + Labda_int_tu * AR_tu2
    dRF_turest        <- k_off * AR_turest - (k_on * A_int_turest * RF_turest/V_int_turest) + Labda_int_turest * AR_turest
    dRF_pro           <- k_off * AR_pro - (k_on * A_int_pro * RF_pro/V_int_pro) + Labda_int_pro * AR_pro
    dRF_li            <- k_off * AR_li - (k_on * A_int_li * RF_li/V_int_li) + Labda_int_li * AR_li
    dRF_spl           <- k_off * AR_spl - (k_on * A_int_spl * RF_spl/V_int_spl) + Labda_int_spl * AR_spl
    dRF_gi            <- k_off * AR_gi - (k_on * A_int_gi * RF_gi/V_int_gi) + Labda_int_gi * AR_gi
    dRF_par           <- k_off * AR_par - (k_on * A_int_par * RF_par/V_int_par) + Labda_int_par * AR_par
    dRF_sm            <- k_off * AR_sm - (k_on * A_int_sm * RF_sm/V_int_sm) + Labda_int_sm * AR_sm
    dRF_lg            <- k_off * AR_lg - (k_on * A_int_lg * RF_lg/V_int_lg) + Labda_int_lg * AR_lg
    #
    list(c(
```

```
dA_ven,
dA_art,

dA_vasc_lu,
dA_int_lu,

dA_vasc_kid,
dA_int_kid,
dAR_kid,
dA_intern_kid,

dA_vasc_tu1,
dA_int_tu1,
dAR_tu1,
dA_intern_tu1,

dA_vasc_tu2,
dA_int_tu2,
dAR_tu2,
dA_intern_tu2,

dA_vasc_turest,
dA_int_turest,
dAR_turest,
dA_intern_turest,

dA_vasc_pro,
dA_int_pro,
dAR_pro,
dA_intern_pro,

dA_vasc_li,
dA_int_li,
dAR_li,
dA_intern_li,

dA_vasc_spl,
dA_int_spl,
dAR_spl,
dA_intern_spl,

dA_vasc_gi,
dA_int_gi,
dAR_gi,
dA_intern_gi,

dA_vasc_par,
dA_int_par,
dAR_par,
dA_intern_par,

dA_vasc_sm,
dA_int_sm,
dAR_sm,
dA_intern_sm,

dA_vasc_lg,
dA_int_lg,
dAR_lg,
dA_intern_lg,

dA_vasc_rm,
dA_int_rm,

dA_vasc_mu,
dA_int_mu,

dA_vasc_sk,
dA_int_sk,

dA_vasc_br,

dA_vasc_ad,
dA_int_ad,

dA_vasc_hrt,
dA_int_hrt,

dA_vasc_bo,
dA_int_bo,

dA_vasc_rest,
dA_int_rest,

dRF_kid,
dRF_tu1,
dRF_tu2,
dRF_turest,
dRF_pro,
dRF_li,
dRF_spl,
dRF_gi,
dRF_par,
dRF_sm,
dRF_lg
```

```
    ))
  })
}


# Observation times
Obs_Times_DCFPYLF18 <- seq(0, 120)

# Regimen
Regimen_DCFPYLF18 <- data.frame(
  var     = "A_ven",
  time    = c(0),
  value   = P_Drug_DCFPYLF18[1, 'Dose_nmol'],
  method  = "add")
Regimen_DCFPYLF18 <- Regimen_DCFPYLF18[order(Regimen_DCFPYLF18$time),]
Events_DCFPYLF18 <- list(data=Regimen_DCFPYLF18)

# Simulation
Simulation_DCFPYLF18 <- lsoda(
                func    = PBPK_Model_DCFPYLF18,
                y       = Initial_DCFPYLF18,
                times   = Obs_Times_DCFPYLF18,
                parms   = P_Model_DCFPYLF18,
                events  = Events_DCFPYLF18
                )
Simulation_DCFPYLF18 <- as.data.frame(Simulation_DCFPYLF18)
```